Pergamon

Geochimica et Cosmochimica Acta, Vol. 62, No. 2, pp. 209–226, 1998
Copyright © 1998 Elsevier Science Ltd
Printed in the USA. All rights reserved
0016-7037/98 $19.00 + .00

PII S0016-7037(97)00335-9

Chemical weathering in a tropical watershed, Luquillo Mountains, Puerto Rico: I. Long-term versus short-term weathering fluxes

ART F. WHITE,[1] ALEX E. BLUM,[1,4] MARJORIE S. SCHULZ,[1] DAVISON V. VIVIT,[1] DAVID A. STONESTROM,[1] MATTHEW LARSEN,[2] SHEILA F. MURPHY,[3,*] and D. EBERL[4]

[1]U. S. Geological Survey, Menlo Park, California 94025 USA
[2]U. S. Geological Survey, Guaynabo, Puerto Rico
[3]Department of Geosciences, The Pennsylvania State University, University Park, Pennsylvania 16802, USA
[4]U. S. Geological Survey, Boulder, Colorado 80303, USA

(*Received June* 19, 1996; *accepted in revised form September* 18, 1997)

Abstract—The pristine Rio Icacos watershed in the Luquillo Mountains in eastern Puerto Rico has the fastest documented weathering rate of silicate rocks on the Earth's surface. A regolith propagation rate of 58 m Ma^{-1}, calculated from iso-volumetric saprolite formation from quartz diorite, is comparable to the estimated denudation rate (25–50 Ma^{-1}) but is an order of magnitude faster than the global average weathering rate (6 Ma^{-1}). Weathering occurs in two distinct environments; plagioclase and hornblende react at the saprock interface and biotite and quartz weather in the overlying thick saprolitic regolith. These environments produce distinctly different water chemistries, with K, Mg, and Si increasing linearly with depth in saprolite porewaters and with stream waters dominated by Ca, Na, and Si. Such differences are atypical of less intense weathering in temperate watersheds. Porewater chemistry in the shallow regolith is controlled by closed-system recycling of inorganic nutrients such as K.

Long-term elemental fluxes through the regolith (e.g., Si = 1.7×10^{-8} moles m^{-2} s^{-1}) are calculated from mass losses based on changes in porosity and chemistry between the regolith and bedrock and from the age of the regolith surface (200 Ma). Mass losses attributed to solute fluxes are determined using a step-wise infiltration model which calculates mineral inputs to the shallow and deep saprolite porewaters and to stream water. Pressure heads decrease with depth in the shallow regolith (-2.03 m H_2O m^{-1}), indicating that both increasing capillary tension and graviometric potential control porewater infiltration. Interpolation of experimental hydraulic conductivities produces an infiltration rate of 1 m yr^{-1} at average field moisture saturation which is comparable with LiBr tracer tests and with base discharge from the watershed. Short term weathering fluxes calculated from solute chemistries and infiltration rates (e.g., Si = 1.4×10^{-8} moles m^{-2} s^{-1}) are compared to watershed flux rates (e.g., Si = 2.7×10^{-8} moles m^{-2} s^{-1}). Consistency between three independently determined sets of weathering fluxes imply that possible changes in precipitation, temperature, and vegetation over the last several hundred thousand years have not significantly impacted weathering rates in the Luquillo Mountains of Puerto Rico. This has important ramifications for tropical environments and global climate change. *Copyright © 1998 Elsevier Science Ltd*

1. INTRODUCTION

Humid tropical ecosystems play an important role in current efforts to characterize worldwide elemental cycles and rates of global carbon sequestration. Tropical ecosystems cover only 25% of the Earth's land surface; yet they are responsible for the global discharge to the sea of 50% of the water, 38% of the dissolved ions, and 65% of the dissolved silica (Meybeck, 1987). Although weathering inputs to relatively large tropical rivers have received considerable attention (Ramirez and Andara, 1993; Suchet and Probst, 1993; Gaillardet et al., 1995), relatively little is known about humid tropical weathering processes in upland watersheds which are responsible for much of the solute and sediment discharge to such river systems (Stallard and Edmond, 1983). Available studies have described mineralogical and chemical changes in weathered tropical regoliths (Eswaran and Bin, 1978; Burnham, 1989; Thomas, 1994) and solute chemistries in stream discharge (Bruijnzeel, 1990; Vegas-Vilarrubia et al., 1994) but have not linked these observations to dynamic processes which control chemical weathering rates and hydrochemical transport.

A recent compilation of solute fluxes from a worldwide distribution of watersheds (White and Blum, 1995) indicates that that the coupled effects of high temperature and precipitation combine to make solute fluxes from the tropical montane environment of the Rio Icacos watershed in Puerto Rico (McDowell and Asbury, 1994), the fastest documented chemical weathering rate of granitoid rocks on the Earth's surface. The present paper characterizes the weathering regimes and reactions within the regolith of Rio Icacos watershed using mass balances based on porewater and stream chemistries and mineralogical changes. These balances are used to calculate both long- and short-term chemical weathering fluxes based on estimates of the age of the regolith and rates of infiltration. A companion paper in this volume (Murphy et al., 1998) discusses specific mechanisms and rates of biotite weathering in the regolith which contributes substantially to solute compositions in the Rio Icacos watershed. Additional studies are ongoing which characterize quartz weathering rates and $^{87}Sr/^{86}Sr$ isotopic distributions.

* Present address: Shepherd Miller Inc., Fort Collins, Colorado 80525, USA

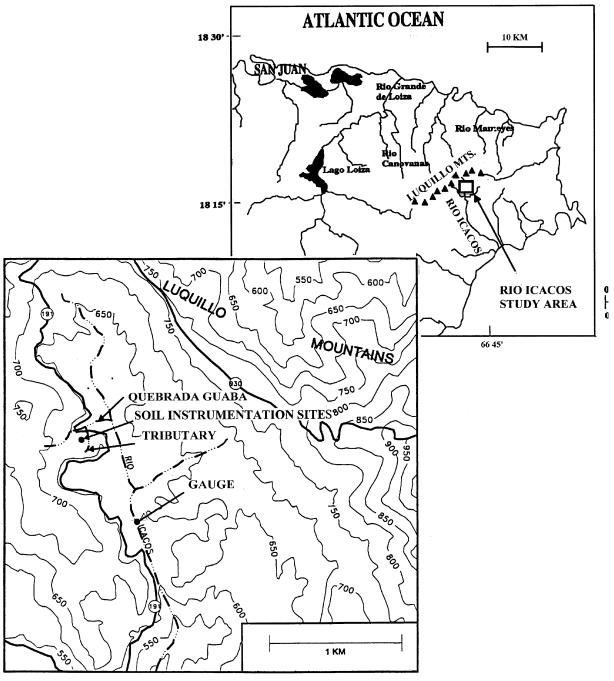

Fig. 1. Maps showing the location of the Rio Icacos watershed and instrumented sites.

2. STUDY AREA

The tropical montane Rio Icacos watershed (Fig. 1) is one of the study areas in the Long Term Ecological Research Program in the Luquillo Experimental Forest (LTER) and is being investigated in the present study as part of U. S. Geological Survey Water, Energy, and Biogeochemical Budgets (WEBB) Program (Larsen et al., 1993). Previous weathering-related studies in this watershed include precipitation chemistry, hydrology, and watershed solute budgets (McDowell et al., 1990; McDowell et al., 1992; and McDowell and Asbury, 1994), regolith development and chemistry (Jones et al., 1982; Zarin and Johnson, 1995), and rates of erosion and mass wasting (Larsen and Torres-Sanchez, 1989; Brown et al., 1995; Larsen, 1997).

The rugged Luquillo Mountains of eastern Puerto Rico (max. elev. 1,074 m) are in the path of the easterly trade winds from the Caribbean and receive most annual rainfall in the form of convective boundary layer storms. The Rio Icacos watershed, located in a lower montane wet colorado forest (*Cyrilla racemiflora*), drains a portion of the southern flank of the Luquillo Mountains (Fig. 1). The watershed area is 326 ha with an elevation range of 600–800 m. Mean annual temperature is 22°C. Average annual rainfall is 4200 mm with strong orographic effects. Detailed weathering studies of the regolith were conducted on the Guaba Ridge, a cuchillo, or knife edge divide on the western side of the Rio Icacos basin which separates two undisturbed first-order streams, the gauged Quebrada Guaba, immediately to the north, and an unnamed stream to the south, called in this study the Quebrada Guaba Tributary (Fig. 1). Both streams discharge into the Rio Icacos.

The watershed is underlain by the Rio Blanco stock, a quartz diorite intrusion of early Tertiary age that crops out over an area of about 25 km^2 (Seiders, 1974). The Rio Blanco stock is medium to coarse grained and is dominated by phenocrysts of quartz and plagioclase with lesser amounts of biotite, hornblende, and K-feldspar, and accessory magnetite, sphene, apatite, and zircon. The shallowest portion of the overlying regolith consist of ultisols which have moderate to high permeability, moderate to low water retention capacity, medium fertility, and rapid runoff (Boccheicamp, 1977). The soil has a total thickness of 50–100 cm and grades from a thin organic-rich A horizon (<10 cm) to a clay-rich basal B horizon. The soil is bioturbated due to burrowing fauna, dominantly earth worms, and root throws. The base of the soil horizon generally corresponds to the maximum depth of root penetration.

Below the soil is a 200–800 cm thick oxidized saprolite which is biologically undisturbed and retains the original bedrock texture. The combined soil and saprolite is referred to as the regolith. This saprolite is similar to those developed elsewhere on granitic rocks in wet mountainous tropical watersheds such as in Malaysia (Burnham, 1989). At the base of the saprolite, a thin transition zone of oxidized slightly-decomposed saprock grades to competent quartz diorite bedrock over an interval of several tens of centimeters. The combined saprock and fresh quartz diorite are referred to as bedrock. Variations in saprolite depth indicate the bedrock does not have a smooth, regular surface but rather consists of core stones formed by weathering along fractures and joints. Hillslope soil and saprolite are generally thinner than on the ridge tops. Landslides on hillslopes are the principal mechanism of physical erosion in the Luquillo Mountains (Larsen and Torres-Sanchez, 1989; Simon et al., 1990).

3. METHODS

The LG soil instrumentation sites are located on the shoulder of the Guaba Ridge. LG-1 is located on the ridge top at an elevation of 680 m (Fig. 1). LG-2 is a hillslope site 20 m down slope from LG-1 on the southern ridge flank, and LG-3 is a site on a steeper part of the ridge shoulder approximately 50 m upslope from LG-1. Each regolith site was instrumented with cup and plate suction water samplers and gas samplers to the point of refusal in the saprock in hand-augered holes and pits (LG-1 <8.5 m; LG-2 <3.3 m; LG-3 <2.3 m). Bulk precipitation and throughfall collectors were installed, and water sampling sites were established on the Quebrada Guaba and the Quebrada Guaba Tributary. Water samples at all sites were collected monthly from 4/92 to 3/94. Samples were filtered in the laboratory, pH, and alkalinity were determined and compositions analyzed using ion chromatography and inductively coupled plasma spectroscopy. Gas samples were analyzed for CO_2 and O_2 using a gas chromatograph with a thermoconductivity detector.

Fresh bedrock samples were collected from a nearby road cut. Regolith cores were obtained at the LG-1 site. Except when noted, all physical and chemical measurements discussed in the paper refer to the LG-1 site. Bulk rock and regolith chemistries were determined by X-ray fluorescence. Qualitative regolith mineralogies were determined by powder X-ray diffraction and thin section. Grain thicknesses of dithionite-treated kaolinite were determined by X-ray diffraction using the methods of Eberl et al. (1996). Compositions of primary plagioclase, K-feldspar, biotite, and hornblende in the quartz diorite and weathered biotite and kaolinite in the regolith were determined by microprobe and mineral abundances were determined by point counting (Murphy, 1995).

Field matric pressures were determined down to depths of 5 m in the regolith using permanently installed porous cup tensiometers equipped with analog vacuum gauges. Bulk density and moisture measurements were made on core samples. Water contents were determined by weight

Table 1. Mineral stoichiometries and abundances (wt %) in the bedrock, soil and saprolite (after Murphy, 1995).

Mineral	Formula	Quartz diorite	Soil 0.17 m	Saprolite 0.76 m	Saprolite 2.87 m	Saprolite 7.13 m
Quartz	SiO_2	24.9	53.7	21.9	23.5	20.6
Plagioclase	$Na_{0.60}Ca_{0.40}Al_{1.36}Si_{2.63}O_8$	56.4	0.0	0.0	0.0	0.0
K-feldspar	$Na_{0.09}K_{0.91}AlSi_3O_8$	1.8	0.0	0.0	0.0	0.0
Biotite (rock)	$K_{0.85}(Al_{0.10}Ti_{0.20}Fe^{2+}_{1.30}Fe^{3+}_{0.05}Mg_{1.25})(Si_{2.8}Al_{1.2})O_{10}(OH)_2$	9.5	NA	NA	NA	NA
Biotite (regolith)	$K_{0.65}(Al_{1.10}Ti_{0.15}Fe^{2+}_{0.35}Fe^{3+}_{0.15}Mg_{0.55})(Si_{3.2}Al_{0.8})O_{10}(OH)_2$	NA	15.7	21.1	18.6	16.2
Hornblende	$(Na_{0.34},K_{0.05})(Ca_{1.71}Mg_{2.84}Fe_{2.06}Al_{0.89}[Al_{1.00}Si_{6.68}]O_{22}(OH)_2$	6.3	0.0	0.0	0.0	0.0
Kaolinite*	$(K_{0.01}Fe_{0.07}Mg_{0.04})(Si_{2.21}Al_{1.69})O_5(OH)_4$	0.0	27.1	57.0	57.9	63.2
Goethite	FeO(OH)	1.9	3.4	2.4	2.5	3.9

* High Si/Al ratios probably reflect qtz contamination.

difference after heating. Moisture saturation (S%) was calculated from porosity and water content. Additional cores through the soil-saprolite interface (29–71 cm) were taken from pits dug adjacent to the LG-1 site and were used in laboratory hydraulic conductivity measurements. Saturated conductivities were measured using a falling head permeameter (Klute and Dirksen, 1986). Unsaturated conductivities were made using steady-state centrifugation (Nimmo et al., 1992).

4. RESULTS

4.1. Mineralogy and Chemistry

Mineral stoichiometries and abundances in the quartz diorite and selective horizons in the regolith are tabulated in Table 1. Plagioclase (An_{40}) and quartz are the dominant silicates in the bedrock with lesser amounts of biotite, hornblende, and alkali feldspar. Mineralogy in the saprolite consists predominantly of primary quartz and biotite and secondary kaolinite and iron oxides, principally goethite. Quartz exhibits triangular and lenticular etch pits on grain surfaces denoting dissolution (Fig. 2a). Similar weathering features have been observed in other tropical weathering environments (Eswaran and Stoops, 1979; Brantley et al., 1986). Altered biotites in the regolith are significantly depleted in K, Mg, and Fe relative to biotite compositions in the quartz diorite (Table 1). As discussed by Murphy et al. (1998), secondary kaolinite forms both as epitaxial growths on plates of this altered biotite (Fig. 2b) as well as in a fine grained matrix which also contains iron oxides. Based on XRD and TEM data, both Murphy et al. (1998) and Dong et al. (1998) concluded that a small portion of randomly interstratified aluminum-hydroxy interlayer vermiculite is present as a alteration product of biotite. Quartz, altered biotite, kaolinite, and iron oxides are present in relatively constant proportions as a function of depth in the saprolite (Fig. 3a). Significant decreases in kaolinite and increases in quartz occur in the overlying soil horizon. Minor K-feldspar and plagioclase persist in only limited amounts in the saprolite and soil (<1%) and exhibit extensive dissolution features (Fig. 2c and d).

The average chemical analysis of bedrock (Table 2) is consistent with the quartz diorite composition reported by Seiders (1974). Relative to bedrock, Na_2O and CaO are completely depleted in the saprolite (Fig. 3b), corresponding to the extensive weathering of plagioclase (Table 1). MgO is depleted and K_2O enriched in the saprolite due to loss of hornblende and retention of biotite. Al_2O_3 and Fe_2O_3 increase with depth in the saprolite due to relative enrichment of kaolinite and goethite. SiO_2 increases and Al_2O_3 and Fe_2O_3 decrease in the overlying soil horizon.

4.2. Hydrology

Porosities, determined from bulk densities and specific gravities (Fig. 4a), are high in the near surface soils at all 3 sites (75% <0.10 m) and decrease with depth to the saprolite-bedrock interface (50% at 0.5 m). This trend corresponds to a progressive decrease in organic matter and translocation of clay from shallower to deeper soil horizons. Porosity is generally constant (~45%) in the underlying saprolite and only decreases at depth near the saprolite-bedrock interface. Graviometric water contents are high through out the regolith and, except in the shallowest soil horizons, do not exhibit significant temporal variations due to intense and evenly distributed precipitation throughout the year (>4000 mm). Undersaturated moisture conditions persist throughout the regolith (Fig. 4b; S = 66–94%) except for saturation (S = 100%) near the saprolite-bedrock interface. Comparable zones of perched groundwater have been described elsewhere in the Rio Icacos watershed (Simon et al., 1990).

The range in pressure heads (Fig. 4c, −0.1 to −2.3 m H_2O), as measured by field tensiometers, is moderately negative (zero corresponds to saturated conditions) and at a fixed depth exhibits only minor variations due to consistent rainfall. Pressures decrease linearly in the soil and upper saprolite horizons (from −0.3 m H_2O at 0.15 m depth to −1.9 m H_2O at 1.5 m depth) indicating that both increasing capillary tension and graviometric potential control pore water infiltration. Pressures again peak at 2.6 m (−0.8 m H_2O) and remain relatively constant to the maximum measured depth (5 m).

Physical and hydraulic properties are reported in Table 3 for core sections obtained from the LG-1 site. Saturated conductivities ranged between 5.5×10^{-6} to 9.5×10^{-5} m s^{-1}. Modest decreases in saturation (100% to 72%) decreased unsaturated conductivities by several orders of magnitude (Fig. 5). The extent of this decrease is greater for the soil cores than for the saprolite core. The range in unsaturated conductivities in the Rio Icacos saprolite (Table 3) is comparable to values reported for other saprolites (1×10^{-9} to 5×10^{-8} m s^{-1}; Schoeneberger et al, 1995; Vepraskas and Williams, 1995).

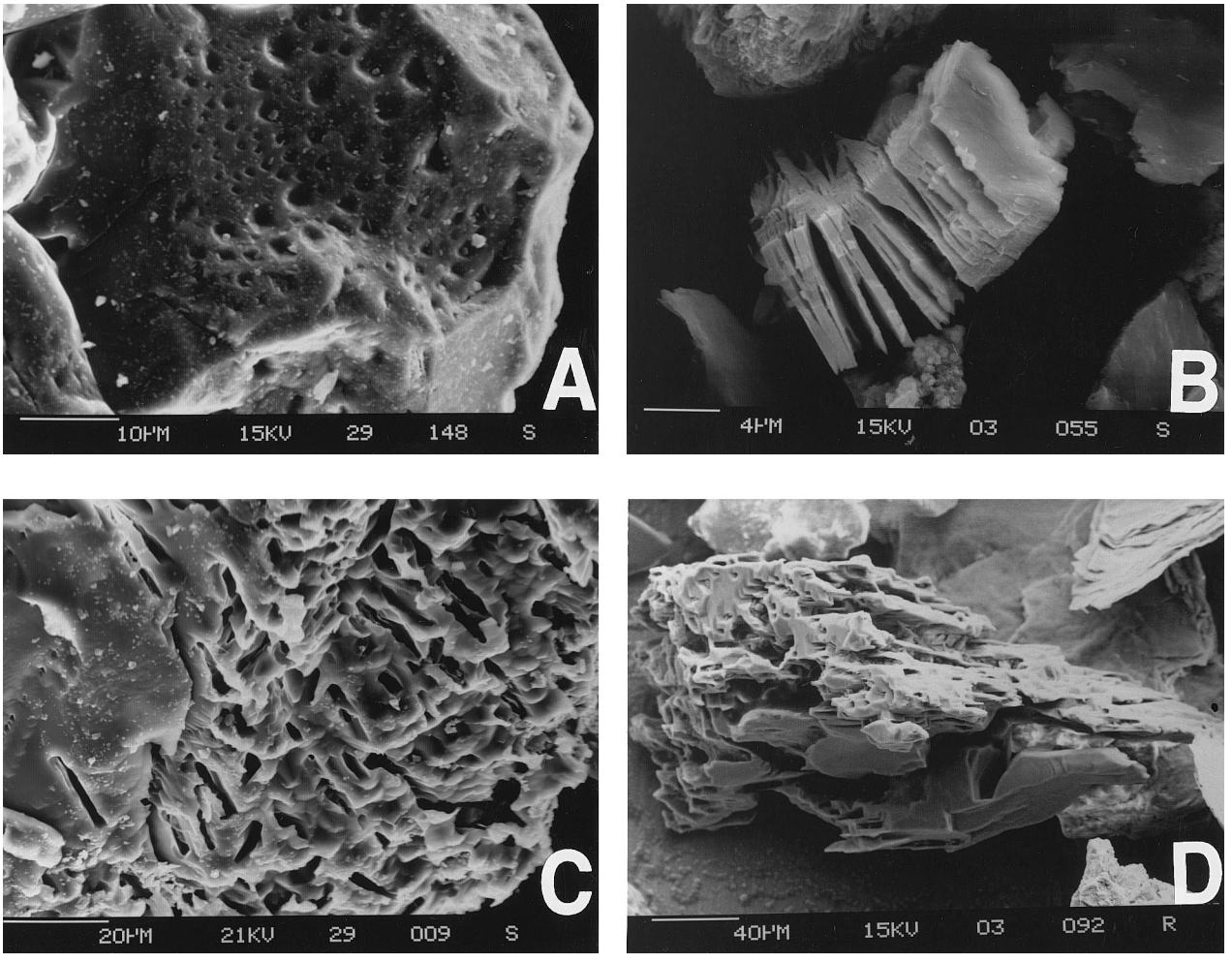

Fig. 2. SEM photos showing weathering textures in the saprolite. (a) Triangular etch pits in quartz at 3.2 m depth. (b) Pseudomorphic replacement of biotite by kaolinite at 1.6 m depth. (c) Elongated intersecting etch pits on a K-feldspar surface at 8.1 m depth. (d) Extensive dissolution features on a plagioclase grain at 1.5 m depth.

4.3. Precipitation Chemistry

Average chemical compositions are reported (Table 4) for open fall and through fall precipitation collected in the Rio Icacos watershed (this study) and for wet precipitation reported from the National Atmospheric Deposition Program (NADP) Station 402020 at El Verde, 10 km from the Rio Icacos (McDowell et al., 1990). Open fall is the sum of solutes derived from both wet precipitation and dry aerosol accumulation under open (treeless) conditions. Wet and open precipitation chemistries in the Luquillo Mountains are dominated by sea salts due to the close proximity to the ocean (McDowell et al., 1990). Solute concentrations are higher in through fall which intercepts the forest canopy. Additional nutrients such as K are leached from leaves and bark and concentrated in through fall by evaporation (Cappellato et al., 1993). Chemical concentrations in all forms of precipitation are relatively constant with time due to a lack of strong climatic seasonality.

4.4. Porewater and Gas Compositions

Average regolith porewater and gas compositions for selected depths at the LG-1, LG-2, and LG-3 sites are tabulated in Table 4. Vertical variations in Cl, Na, Ca, K, Mg, and Si, are shown in Fig. 6 for samples from the LG-1 ridge top site. The soil porewaters ($<$0.5 m) exhibit both higher concentrations and greater variability than porewaters in the underlying saprolites. The majority of plant roots are confined to the soil horizon and enhance evapotranspiration and cycling of inorganic nutrients (Brown et al., 1983). Porewaters in the upper saprolite ($<$2 m) are more dilute with average Cl/Na ratios (1.09) similar to seawater (1.17). Concentrations approximate a mixture of open and through fall precipitation (vertical dashed lines, Fig. 6), implying that a significant portion of infiltration to the saprolite bypasses evaporative concentration in the soil through macropore flow along root casts and animal burrows during frequent recharge events.

Chlorine, sodium, and calcium exhibit no significant changes in concentration with depth in the saprolite compared to Si, K, and Mg which increase linearly with depth (Fig. 6). Regression fits predict that an average of 28 μM of Si, 5 μM of K, and 8 μM of Mg are leached into the porewater during infiltration through 1 m of saprolite (Table 5). Although compressed into thinner sequences, solute trends in LG-2 and LG-3 sites are

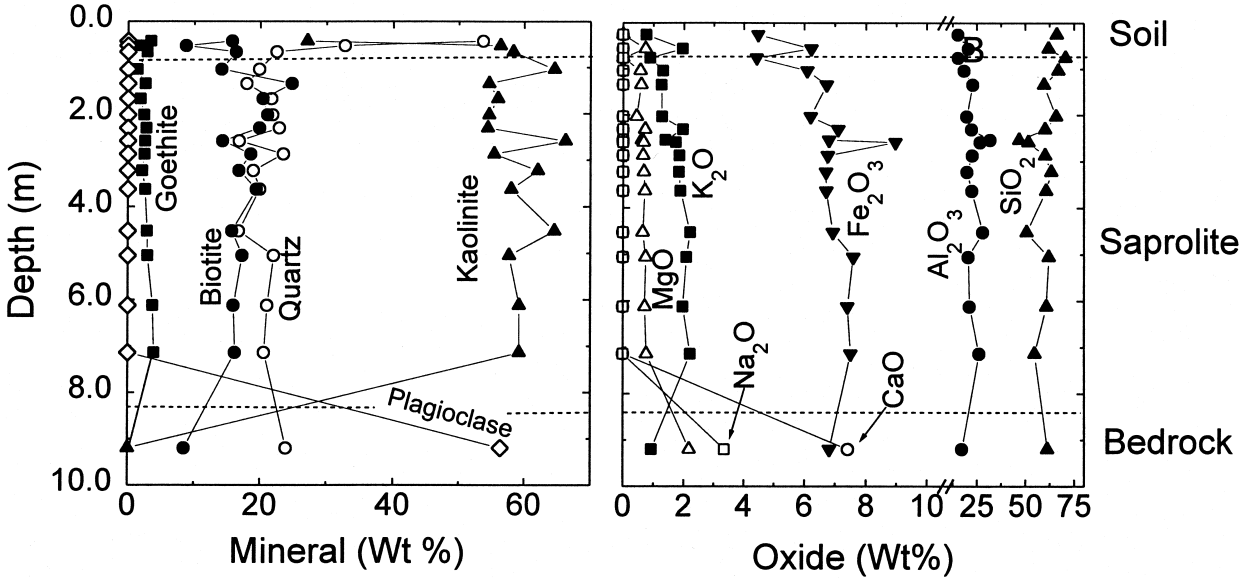

Fig. 3. Wt% of minerals and oxides in the regolith profile.

similar. Higher solute concentrations occur at the base of the LG-2 saprolite compared to the rest of the profile, reflecting water movement along the saprolite-bedrock interface from upslope drainage. The lateral movement of solutes, such as Si, along hillslope landscapes is an important feature of tropical pedogenesis (Millot et al., 1976).

CO_2 partial pressures in the regolith (Table 4, 3.1–6.0 vol%) reflect root transpiration and rapid microbial oxidation of organic carbon in the soil horizon. No CO_2 gradient is evident in the regolith indicating that the rate of CO_2 production at shallow rooting depths, coupled with downward diffusion through the permeable saprolite is sufficient to overcome CO_2 loss to the atmosphere and CO_2 consumption by silicate hydrolysis at depth. The O_2 partial pressures indicate oxic conditions throughout the regolith.

Table 2. Bedrock and regolith chemistry (data in wt% except as noted).

	Quartz diorite	Soil 0.17 m	Saprolite 0.76 m	Saprolite 2.87 m	Saprolite 7.13 m
SiO_2	61.20	66.13	70.67	60.12	54.74
Al_2O_3	17.20	15.22	15.35	22.59	26.14
Fe_2O_3	6.81	4.47	4.42	6.76	7.50
MgO	2.18	0.00	0.00	0.65	0.76
CaO	7.24	0.00	0.00	0.00	0.00
Na_2O	3.35	0.00	0.00	0.00	0.00
K_2O	0.93	0.76	0.88	1.85	2.21
TiO_2	0.49	0.43	0.39	0.47	0.56
P_2O_5	0.13	0.00	0.00	0.00	0.00
MnO	0.18	0.01	0.02	0.05	0.57
Zr[1]	60	163	106	108	93
Y[1]	26	22	17	15	20
Nb[1]	4	10	9	6	9
Sr[1]	290	37	27	22	22
Density	2.70	0.84	1.29	1.27	1.22

[1] ppm.

4.5. Surface Water Compositions

Average solute chemistries of the Rio Icacos, Quebrada Guaba, and Quebrada Guaba Tributary streams are similar, dominated by Na, Ca, Si, and bicarbonate alkalinity (Table 4). Specific differences in concentrations are attributed to varying inputs from surface runoff, porewater and groundwater. Average solutes in the Quebrada Guaba Tributary are compared to LG-1 pore waters in Fig. 6 (SW-vertical dashed lines). Stream Cl is generally similar to porewaters suggesting that ET is not a major process concentrating solutes in the stream waters. Average watershed evapotranspiration is 17% (McDowell and Asbury, 1994). Stream water Ca, Na, and Si concentrations are higher and K and Mg concentrations are lower than in porewaters in the deep saprolite.

5. DISCUSSION

Chemical weathering in the Rio Icacos watershed can be characterized in terms of both weathering intensity and rate. Weathering intensity, sometimes referred to as grade or index in tropical soils (Van Wambeke, 1962; Thomas, 1994), relates to the degree of mineralogical and chemical depletion of primary and secondary minerals in the regolith. The weathering rate is a kinetic term which temporally defines the rapidity with which this depletion occurs. Weathering rates are determined either by integration over long-term changes in regolith mineralogy and chemistry or by calculation of short-term solute fluxes in regolith porewaters or in watershed discharge.

The relationship between weathering intensities and weathering rates is dependent on a number of complex interactions. The role of chemically limited vs. physically limited weathering environments, as defined by Stallard and Edmond (1983) plays an important role in selective mineral weathering and on weathering intensities and rates. Average physical denudation rates in the Rio Icacos watershed range from approximately 25 to 50 m Ma^{-1} for the relatively stable ridge tops (Brown et al.,

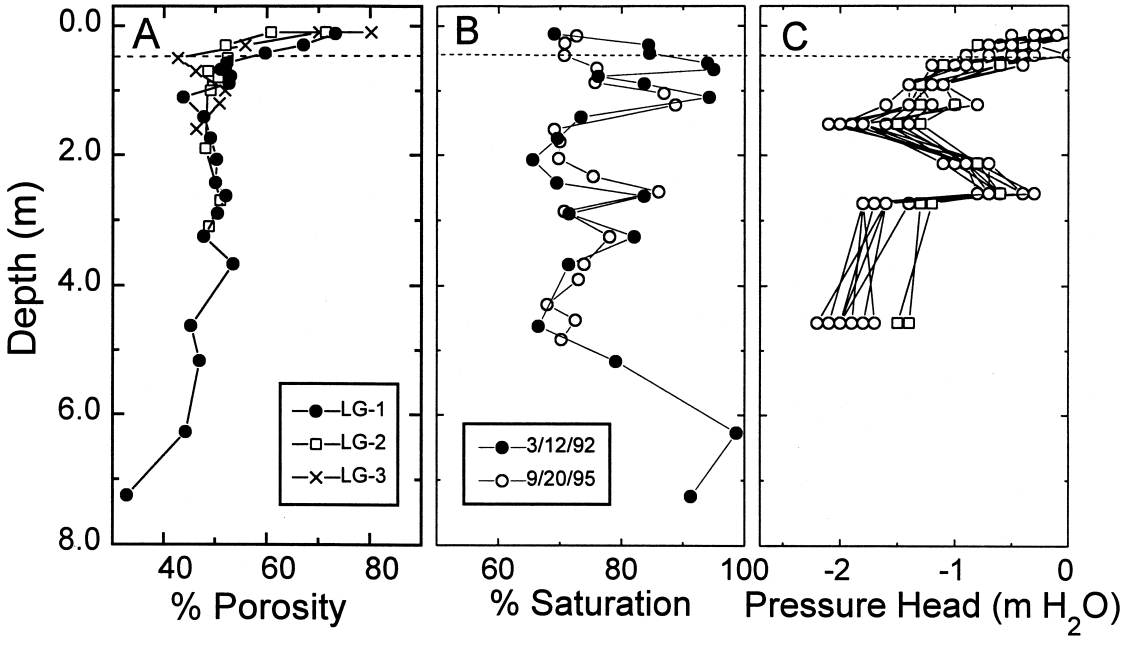

Fig. 4. Physical and hydrologic characteristics of the regolith: (a) porosity, (b) moisture saturation, and (c) pressure heads. Dashed horizontal line is the depth of the soil/saprolite interface.

1995) upwards to between 60 and 600 m Ma^{-1} for local hill slopes dominated by periodic landslide events (Larsen, 1997). These denudation rates are very fast compared to cratonic provinces on which many tropical soils develop (1 m Ma^{-1}; Thomas, 1994). In the chemically limited weathering regime of the Rio Icacos, reactive minerals, such as plagioclase and hornblende, are readily accessible to chemical weathering at the bedrock-saprolite interface and less reactive primary silicates such as biotite and quartz are weathered in the overlying regolith (Fig. 3b).

In addition to steep topography and high denudation rates, the weathering environment in the Rio Icacos watershed is subjected to extremely high rain fall (4200 mm) and tropical temperatures (22°C). High precipitation is expected to promote weathering by increasing wetted mineral surface areas and by decreasing porewater chemical concentrations and reaction affinities (Velbel, 1993). Higher temperatures are assumed to increase silicate reactions via the Arrhenius temperature relationship (Brady, 1991).

5.1. Intensity of Chemical Weathering

Weathering in the Rio Icacos watershed is of moderate intensity. The preservation of biotite in the saprolite contrasts with more intense weathering in stable tropical shield areas, such as Venezuela and Columbia, where primary aluminosilicates, including biotite, are completely weathered out at the granite-saprolite interface (Edmond et al., 1995). In temperate

Table 3. Physical and hydraulic properties of cores from the LG-1 site.

	Conductivity k_m (m s^{-1})	Water content (m^3 m^{-3})	Pressure head (m H_2O)	Bulk density (Mg m^{-3})	Moisture saturation (%)
Soil #1	6.3E-06	0.46	0.00	1.19	100
0.32 m[1]	1.2E-07	0.39	−1.34	1.23	88
	1.6E-08	0.38	−2.47	1.25	88
	1.9E-09	0.35	−6.43	1.28	85
Soil #2	9.5E-05	0.35	0.00	1.24	100
0.32 m[1,2]	1.9E-07	0.32	−1.44	1.35	88
	2.5E-08	0.30	−2.10	1.37	88
	1.0E-09	0.25	−3.14	1.37	84
Upper Saprolite	5.5E-06	0.43	0.00	1.19	100
0.68 m[1]	1.0E-07	0.37	−0.01	1.33	98
	2.8E-08	0.32	−0.02	1.33	89
	5.0E-09	0.26	−0.07	1.35	72

[1] At midpoint; cores were 3 to 6 cm long.
[2] Duplicate core.

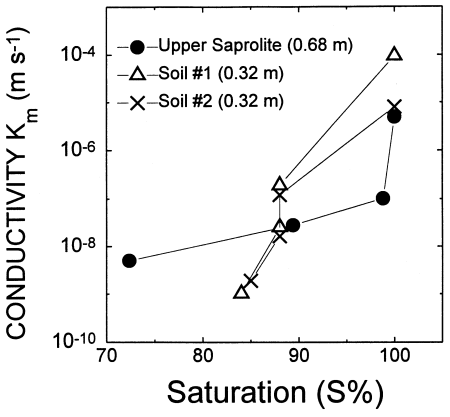

Fig. 5. Experimental hydraulic conductivities for differing moisture saturation in soil and saprolite cores.

zone saprolites, more diverse assemblages of primary mineral persist, implying a lower intensity of chemical weathering. Saprolite profiles described by Pavich (1989) in Virginia, for example, contain significant plagioclase in lower 10 m of the section whereas both biotite and K-feldspar are preserved in a 4 m thick section of saprolite on quartz diorite at Panola Mountain, Georgia (White et al., 1998).

The intensity of weathering is reflected by chemical differences between porewater and stream water in a watershed. In low intensity weathering, a greater proportion of the primary silicates are preserved in the regolith and both porewaters and stream waters reflect dissolution of the most reactive primary phases. This is the case for the temperate watersheds in which comparable average Ca and Si concentrations in porewaters and stream water reflect predominantly plagioclase weathering (Fig. 7). In contrast, Si and Ca concentrations are much lower in the Guaba Ridge saprolite porewaters relative to the Rio Icacos stream water. More intense weathering at the saprolite-bedrock interface has effectively depleted plagioclase from the overlying regolith, producing porewaters that are deficient in Ca and Si. These contrasting chemistries signify a fundamental difference in the regolith and bedrock weathering regimes in tropical watersheds.

The predominance of secondary kaolinite throughout the Rio Icacos regolith (Fig. 3a) also reflects moderate weathering intensity in contrast to the prevalence of aluminum and iron oxides in more intensely weathered SiO_2-depleted laterites and bauxites on stable tropical granite terrains (Nahon, 1991). Kaolinite stability is reflected by Al_2O_3 conservation in the Rio Icacos regolith (Fig. 3b) and in low Al concentrations in porewaters. Measurable total dissolved Al occurs predominantly in the shallow porewaters (Fig. 8) and correlates with higher dissolved organic contents (max. DOC = 2.5 mg l^{-1}, Murphy, 1995). Both Al and DOC are commonly below detection limits (0.5 μM and 0.1 mg l^{-1}, respectively) at depths >2.0 m.

Solubility calculations (SOLMINEQ.88; Kharaka et al., 1988) using total dissolved Al concentrations produce ionic activity products (IAP) that exceed saturation values for kaolinite (K_s) by up to 8 orders of magnitude (Fig. 9, closed symbols). Excessive supersaturation stems from complexation of Al at low concentrations, particularly at near-neutral pH (Huges et al., 1994; Berggren and Mulder, 1995). Corrections for complexation, based on assumed equilibrium between monomeric Al^{3+} concentrations and amorphous gibbsite saturation (Karathanasis, 1989; Norfleet et al., 1993) produced kaolinite IAPs that were independent of pH and averaged an order of magnitude above kaolinite saturation (Fig. 9, open symbols). This supersaturation is compatible with the kinetics associated with kaolinite precipitation from solution (Nagy et al., 1991).

Grain morphologies also reflect the relative stability of ka-

Table 4. Average chemical compositions of precipitation, pore waters, surface waters and gases.*

	Precipitation			Regolith							Surface water		
	LGRC 1 open fall	LGRC3 thru fall	El Verde wet[1]	LG1 0.9 m	LG1 1.2 m	LG1 8.5 m	LG2 0.9 m	LG2 3.6 m	LG3 0.9	LG3 2.2 m	Rio Icacos[2]	Quebrada Guaba	Tributary Quebrada
pH	5.6	5.2	5.1	4.9	4.0	5.1	4.5	5.4	4.9	5.2	6.8	6.5	6.5
Na	59.2	119	66.0	204	90.2	156	138	220	292	204	222	250	261
K	1.4	12.3	1.8	6.0	5.2	39.5	4.7	16.7	9.4	7.3	13.0	11.5	18.1
Ca	3.8	6.8	4.2	12.1	12.7	27.2	4.5	14.3	11.8	13.5	83.0	73.0	107
Mg	6.8	13.2	7.5	24.4	18.9	59.3	12.6	50.2	48.0	38.4	49.0	44.4	47.2
Li	0.0	0.0	nd	5.7	0.0	4.3	0.4	0.1	0.7	13.6	nd	0.4	0.0
Mn	0.0	0.0	nd	1.4	0.2	3.6	0.2	0.9	0.9	3.3	nd	0.0	0.0
Fe	0.0	0.0	nd	0.2	0.0	0.3	0.0	0.2	0.4	0.6	nd	0.4	0.0
Al	0.0	0.0	nd	3.4	9.0	15.6	3.2	6.8	5.1	6.5	nd	0.0	0.2
Si	0.0	0.0	nd	61.1	60.7	216	52.5	115	75.0	147	305	323	424
Sr	1.9	0.0	nd	0.1	0.3	0.1	0.0	0.0	0.1	0.1	nd	0.18	0.20
Alk	0.0	0.0	nd	16.4	0.0	67.6	4.8	34.3	7.5	38.0	347	323	420
Cl	64.9	163	82.0	246	128	171	152	217	262	212	176	193	177
NO_3	0.0	0.0	4.3	6.2	0.0	18.9	4.8	12.2	11.3	17.9	50.0	2.5	2.9
SO_4	6.9	15.4	8.5	11.0	12.4	7.6	3.1	24.8	42.9	2.2	23.5	10.6	13.3
CO_2*	nd	nd	nd	4.8	3.1	3.8	nd	nd	6.0	3.7	nd	nd	nd
O_2*	nd	nd	nd	16.2	24.0	18.3	nd	nd	nd	nd	nd	nd	nd

* Units are in μM except as noted.
[1] McDowell et al., 1990.
[2] McDowell and Asbury, 1994.
* gases are vol.%.

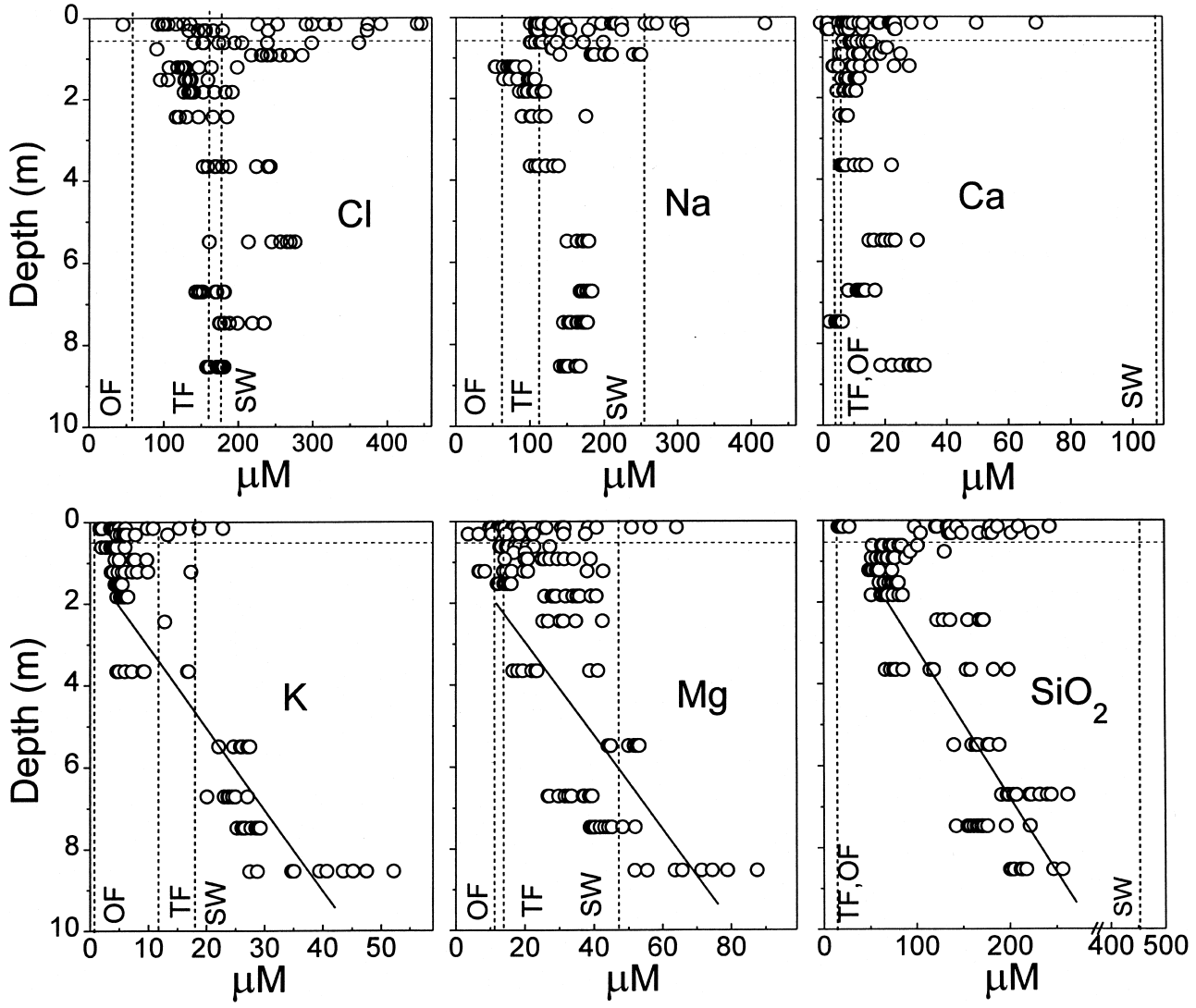

Fig. 6. Porewater concentrations as functions of depth at the LG-1 ridge top site. Dashed horizontal line is the depth of the soil/saprolite interface. Vertical dashed lines correspond to average solute concentrations for open fall (OF), through fall (TF) and stream water in the Quebrada Guaba Tributary (SW). Solid lines correspond to linear regression fits through the porewater K, Mg, and Si data as functions of depth in the saprolite (Regression data reported in Table 5).

olinite in the regolith profile. X-ray scattering domains perpendicular to the (001) crystallographic direction were used to determine the average thickness of matrix kaolinite, i.e., <2 μm size which excludes biotite pseudomorphs (Eberl et al., 1996). These thicknesses may correspond directly to dimensions of individual kaolinite grains or to particles composed of several crystallographic domains with subgrain boundaries (Eberl et al., 1997). Below ~1 m depth, grain size distributions are relatively constant with mean thicknesses varying between 6 and 8 nm (Fig. 10a). The size distributions are log-normal (Fig. 10b), suggesting that kaolinite precipitated by a surface controlled mechanism under open system conditions (Eberl et al., 1997). This is consistent with Al and Si supplied by weathering of primary silicates at the bedrock-saprolite interface. The consistent mean size and shape of the particle distributions between 1 m and 7 m suggests minimal kaolinite precipitation or dissolution in the saprolite matrix.

Table 5. Correlations between saprolite pore water chemistry and depth, concentration (μM) = $a_0 + a_1 *$ Depth (m).

Element	Intercept a_0	Slope a_1	Correlation r^2
Si	14.9	27.6	0.74
K	−5.4	5.1	0.81
Mg	−4.8	8.2	0.47
Ca	na	na	0.11
Na	na	na	0.09
Cl	na	na	0.09

na = no apparent relationship between concentration and depth.

Above 1 m in the regolith, kaolinite particles are thicker (8–9 nm) and the grain size distributions suggest fewer particles in

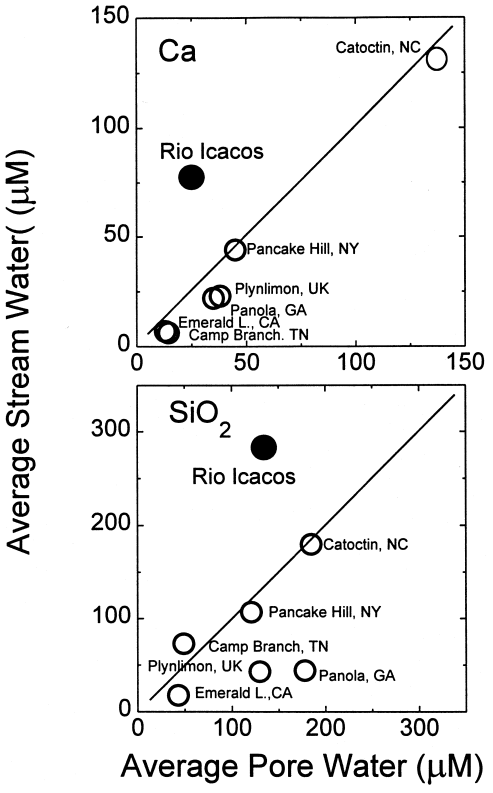

Fig. 7. Average Ca and Si concentrations in porewater and surface waters for the tropical Rio Icacos watershed (solid symbol) and temperate watersheds (open symbols). Diagonal line is a direct correlation. Data is for Camp Branch (Kelly et al., 1988), Catoctin (Katz et al., 1989), Panola, (White et al., 1998), Plynlimon (Durand et al., 1994), and Emerald Lake (Hooper and Peters, 1993).

the finer size fractions. This is consistent with the preferential dissolution of fine kaolinite particles in the shallow biologically active zone. It is likely that the higher DOC values in the near surface, which promote mobilization of Al (Fig. 8, Murphy, 1995), also results in the dissolution of kaolinite. The preceding observations suggest kaolinite is thermodynamically stable with respect to saprolite porewaters below the biologically

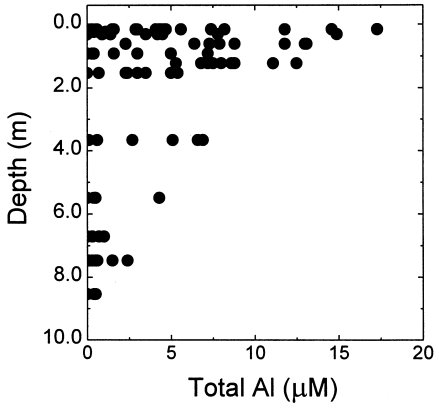

Fig. 8. Distribution of total dissolved Al (<0.45 μm) in porewaters with depth.

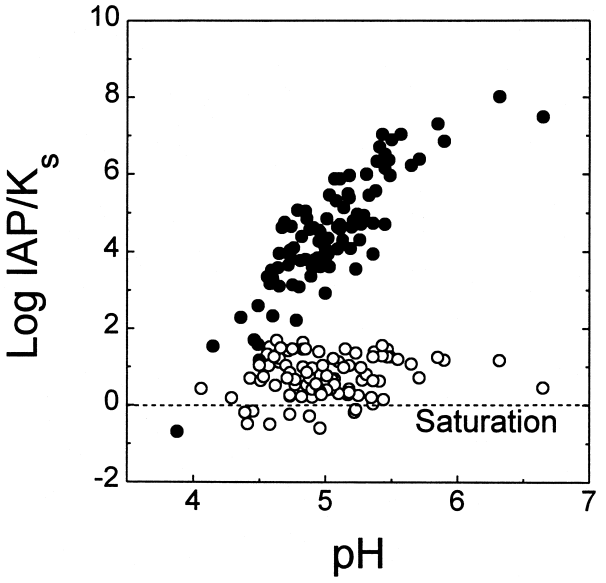

Fig. 9. Ratios of ionic activity product (IAP) to kaolinite solubility K_s for porewaters as functions of pH. Closed circles are IAP/K_s based on total analyzed Al, and open circles are values based on Al equilibrium with gibbsite.

active region and is the principal secondary mineral defining weathering intensity in the Rio Icacos saprolite.

5.2. Rates of Chemical Weathering

In contrast to moderate weathering intensities, weathering rates in the Rio Icacos watershed are extremely rapid. Based on solute weathering fluxes (McDowell and Asbury; 1994), White and Blum (1995) concluded that the Rio Icacos watershed has the fastest documented watershed weathering rate of granitoid rocks on the Earth's surface. The weathering flux of Si (8000 mole ha^{-1} yr^{-1}), for example, exceeds 2000 mole ha^{-1} yr^{-1} on granitic terrain in Malaysian tropical rain forests (Vegas-Vilarrubia et al., 1994) and 1500 mole ha^{-1} yr^{-1} for comparable rocks in temperate rain forests of British Columbia (Zeman, 1975).

5.3. Contributions of Weathering to Porewater Compositions

Porewater solute fluxes occur within a smaller spatial scale than watershed fluxes and can provide a more accurate assessment of weathering rates. The relatively flat topography on top of the Guaba ridge decreases the impact of high physical erosion rates and allows for the assumption of one dimensional hydrologic transport through the regolith. The rate of change in solute concentrations with regolith depth (Fig. 6 and Table 5) can be used to quantify the magnitude and rate of weathering reactions. The chemical perturbations caused by nonweathering processes, including seasonal variations in moisture content (Chartes, 1990) base cation exchange (Kirkwood and Nesbitt, 1991) and biological cycling (Velbel, 1995) need to be taken into account. Compared to temperate sites, the first two processes are minimized in the Rio Icacos watershed due to a lack of seasonality in precipitation, low evapotranspiration, and low

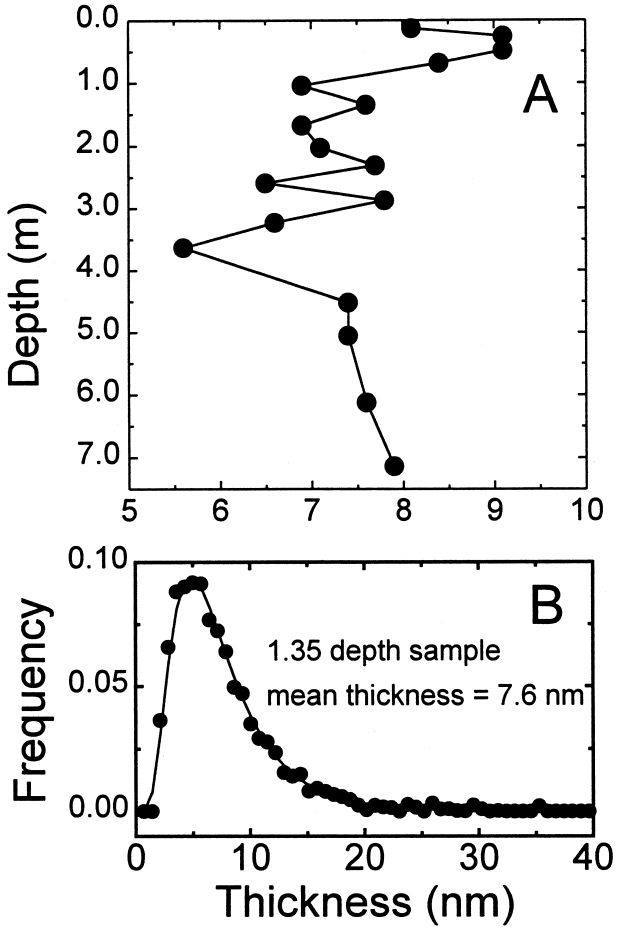

Fig. 10. (a) Mean thickness (perpendicular to the basal plane) of fine grained kaolinite (<2 μm) as a function of depth at the LG1 site. (b) Crystal size distribution of the 135 cm depth sample which is typical of samples from >1 m, and the best fit theoretical log-normal distribution (solid line).

cation exchange capacities of the kaolinitic regolith. However, as will be discussed in greater detail, porewater compositions are impacted by cycling of inorganic macronutrients such as K, Mg, and Ca through the shallow rain forest soils.

Weathering during infiltration is modeled as a step-wise mass-balance process. This approach requires defining the interfaces from which mass balances will be calculated, compositions of the input and output solutions (Fig. 11, solid boxes) and relevant mineral weathering reactions (Fig. 11, dashed boxes). The interfaces are: (1) the top of the shallow saprolite which integrates chemical inputs from open fall, through fall and the soil, (2) the base of the deep saprolite which integrates chemical inputs between the shallow saprolite to the bedrock interface, and (3) the stream which reflects a mixture of shallow and deep saprolite porewater that has been modified by weathering at the saprolite-bedrock interface. The respective chemistries are defined at 1.2 m and 8.5 m in the regolith and by the Quebrada Guaba Tributary (Table 4).

A total fluid mass (1000 g) is conserved in the calculations and is apportioned during mixing and evapotranspiration based on solute Cl concentrations (Fig. 11, arrows), which are not significantly impacted by mineral weathering (Table 1). Results indicate that 360 g of open fall and 640 g of through fall produce the observed solute Cl at the top of the saprolite. The evapotranspiration loss in the overlying soil is assumed to be incorporated into the two precipitation terms. The subsequent increase in Cl in the deeper saprolite reflects an additional loss of 220 g of water to evapotranspiration. Average surface water composition is composed of 60% shallow saprolite water (470 g) and 40% deep saprolite (310 g). No additional evaporation is assumed to occur in the surface water.

Mineral weathering contributions to changes in porewater concentration Δc_j are defined by the mass balance relationship (Velbel, 1986)

$$\Delta c_j = \sum_{m=1}^{\phi} \Delta C_m \beta_{j,m} \quad j = 1 \cdot \cdot n \tag{1}$$

where ΔC_m is the mass of mineral m reacted (positive for dissolution and negative for precipitation), and $\beta_{j,k}$ is the stoichiometric factor describing the distribution of element j in m. The sequence of linear simultaneous equations is solved using the NETPATH computer program (Plummer et al., 1991). The calculations are constrained by the number of elements and minerals considered (n and ϕ) and changes in the mass of water due to mixing and evaporation. The larger the number of constraints that can used to uniquely define a solution, the lower the uncertainty in describing the weathering process.

Reactions involving primary and secondary minerals in the soil and saprolite horizons are described by two sets of constraints, K-Ca-Fe-Si-Al-Cl and Mg-Ca-Fe-Si-Al-Cl (Fig. 11, boxes A and B). Each set contains four of the five elements which comprise the dominant mineral phases in the regolith, i.e., biotite, quartz, kaolinite, and goethite (Fig. 3A). Incorporation of additional constraints into a single mass balance calculation was not possible because solutions to Eqn. 1 became over-determined.

Calculations of weathering inputs at <1.2 m produced contradictory results (Fig. 11, dashed box A) with the K-Fe-Si-Al-Cl constraints predicting kaolinite dissolution (11 μM) and biotite precipitation (-5 μM) and the Mg-Fe-Si-Al-Cl constraints predicting kaolinite precipitation (-12 μM) and biotite dissolution (15 μM). These inconsistencies are produced by the depletion of K in the shallow saprolite porewater at 1.2 m relative to the input mixture of through fall and bulk precipitation. This triggers the unrealistic precipitation of biotite (-5 μM) when using the K-Fe-Si-Al-Cl constraints. Other studies (Roda et al., 1990; Bain et al., 1994) have shown that soil porewater K concentrations are often lower than in through fall due to K uptake by vegetation. Other nutrient budgets in the Luquillo Mountains have shown that chemical weathering produces only a small portion (10–40%) of the total K, Ca, and Mg cycled through the shallow soils (Jordon et al., 1972).

In contrast to the shallow regolith, both the K-Ca-Fe-Si-Al-Cl and Mg-Ca-Fe-Si-Al-Cl constraints produce consistent changes in solute compositions between the top (1.2 m) and bottom (8.5 m) of the saprolite (Fig. 11, dashed box B). The dissolution of 38 μmoles of biotite produces the K increase while 50 μmoles of biotite produces the Mg increase. The significant increases in Si (Fig. 6) result from both biotite (38 and 50 μmoles) and quartz (61 and 52 μmoles) dissolution.

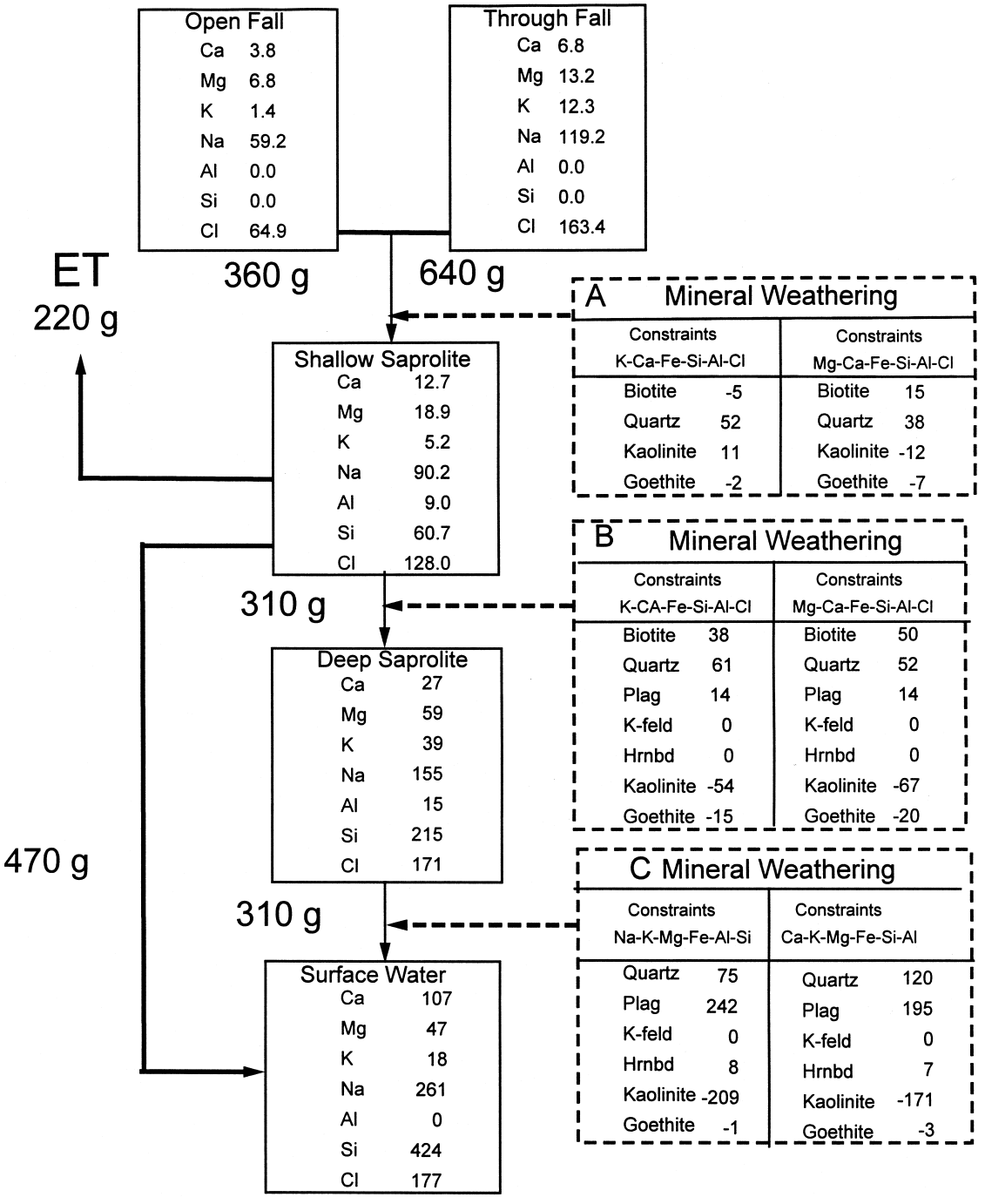

Fig. 11. Schematic describing mineral and fluid fluxes in the Rio Icacos regolith. Solid arrows are water transfers due to infiltration, mixing and evapotranspiration. Dashed arrows are mineral inputs. Solid boxes are solute concentrations (μmoles $\cdot$ kg^{-1} H_2O) and dashed boxes are masses of minerals reacted (μM) under different model constraints, ([−] = dissolution and. [+] = precipitation).

Equal but small amounts of plagioclase (14 μmoles) are dissolved under both constraints (the only source of solute Ca in the saprolite is plagioclase). All of the Al produced by biotite and plagioclase dissolution is incorporated into kaolinite (54 and 67 μmoles), and all the Fe is incorporated into goethite, (15 and 20 μmoles) which is in agreement with very low concentrations of these species in the saprolite porewaters.

A shallow biologically-dominated soil porewater overlying a weathering-dominated saprolite porewater, as predicted by the above calculations, is consistent with the concept of open and closed nutrient cycles in tropical ecosystems (Burnham, 1989). In a closed-system, inputs of inorganic nutrients from weathering are negligible, and forest fertility is maintained by low level atmospheric inputs and by efficient retention and recy-

cling of those nutrients in near-surface soil horizons. In Malaysia, nutrient balances in the soils were found constant and invarient to significant differences in the chemical composition of the underlying saprolite and bedrock (Hamdan and Burnham, 1996). Even Si is rapidly cycled at shallow depth in some tropic rain forest environments (Lucas et al., 1993). In an open-system, there are significant inputs of nutrients from weathering at depth. In contrast to the Rio Icacos regolith, White et al. (1998) observe a lack of consistent increases in porewater macronutrients such as K, Ca, and Mg with depth in saprolites in the subtropical Panola Research Watershed in Georgia USA. The authors ascribe this to open-system uptake of these nutrients during weathering by roots which penetration to depths > 4 m.

Stream water compositions in the Rio Icacos watershed represent a mixture of shallow and deep pore waters (Fig. 11). Stream water is also characterized by significant increases in Ca, Na, and Si reflecting dissolution of plagioclase at the bedrock interface. Two sets of weathering constraints, Ca-K-Mg-Fe-Al-Si and Na-K-Mg-Fe-Al-Si (Fig. 11, dashed box C) each contain two of the three elements (Ca, Na, and Si) most dependent on plagioclase dissolution. The Na-K-Mg-Fe-Si-Al constraints predict that 242 μmoles of plagioclase dissolve while the Ca-K-Mg-Fe-Al-Si constraints predicted that 195 μmoles dissolve. The volumetric loss of plagioclase at the bedrock interface is a common feature of tropical weathering of granitoid rocks and is primarily responsible for the mechanical degradation of the bedrock that forms the porous and friable saprolite (Thomas, 1994). This physical disintegration, induced by chemical weathering, is termed ''arenisation'' and is an important initial stage of weathering of granite in tropical environments (Millot, 1970; Eswaran and Bin, 1978).

Both the Ca-K-Mg-Fe-Al-Si and Na-K-Mg-Fe-Al-Si constraints predict that small amounts of quartz and hornblende and no K-feldspar or biotite dissolve to produce stream water compositions (Fig. 11, Box C). The lack of K-feldspar dissolution agrees with low concentrations in the bedrock (1.8%, Table 1) Most biotite is preserved during bedrock rock weathering and is subsequently weathered in the saprolite. More kaolinite is formed from plagioclase and hornblende dissolution at the saprolite-bedrock interface (171–209 μmoles, Box C)) than from subsequent biotite weathering in the saprolite (54–67 μmoles, Box B). This dual paragenesis is reflected by differences in kaolinite morphology. Fine-grained plasmogenic kaolinite is produced by plagioclase weathering. Grain size distributions (Fig. 10) suggest that, except in the shallow soils, this kaolinite is stable in the overlying saprolite. Additional kaolinite produced during weathering in the saprolite is present as pseudomorphic replacement of altered biotite as shown in Fig. 2b.

5.4. Regolith Chemistry and Long-Term Weathering

Changes in porewater solutes are produced by extremely small changes in mineral abundances over hydrologic residences times. However, on the time scale of regolith development, solid state mass losses are significant and are indicative of average long term weathering rates. The most common approach to quantify such weathering is to ratio the concentration of a chemical species j in the regolith $C_{j,w}$ to that in the underlying protolith or bedrock $C_{j,p}$. The ratio, as defined by Brimhall and Dietrich (1987), Chadwick et al. (1990), and Merritts et al. (1992)

$$\frac{C_{j,\mathrm{w}}}{C_{j,\mathrm{p}}} = \frac{\rho_\mathrm{p}}{\rho_\mathrm{w}} \frac{1}{(\epsilon + 1)} (1 + \tau_j) \tag{2}$$

is dependent on changes in protolith/regolith densities $\rho_\mathrm{p}/\rho_\mathrm{w}$, and volume changes described by the strain factor ϵ_j where $\epsilon_j = V_\mathrm{w}/V_\mathrm{p} - 1$. Together density and strain are described as closed-system contributions which occur without movement of the component under consideration (i.e., $C_{j,\mathrm{w}}$). The mass transfer coefficient τ_j is an open-system contribution that describes mass movement of element j across the unit regolith volume (m^3). When $\tau_j = -1$, the mass of element j is completely lost during weathering. If $\tau_j = 0$, j is immobile and is only affected by closed chemical system processes.

5.5. Rates of Iso-Volumetric Weathering

The volumetric strain in Eqn. 2 can be calculated from the ratios of densities and concentrations of an inert element i in the regolith and bedrock such that

$$\epsilon_j = \frac{\rho_\mathrm{p} C_{i,\mathrm{p}}}{\rho_\mathrm{w} C_{i,\mathrm{w}}} - 1 \tag{3}$$

The density ratio $\rho_\mathrm{p}/\rho_\mathrm{w}$, in the LG-1 profile is greatest in the soil ($<$0.5 m) due to higher organic content and bioturbation (Fig. 12a). The underlying saprolite maintains a relative constant density ratio of 2.0 (50% porosity). Conservative elements defined in Eqn. 3 may include Zr, (Harden, 1987; Chadwick et al., 1990), Ti (Johnson et al., 1968), and rare earth elements such as Nb and Y (Brimhall and Dietrich, 1987). Zirconium, titanium, and niobium produce consistent estimates for strain ϵ_j which center close to zero (Fig. 12b, vertical dashed line). Lack of a significant volume change indicates that weathering is essentially iso-volumetric, which is consistent with a porosity of nearly 50%, and with the preservation of primary granitoid textures in the saprolite. Such isovolumetric weathering is a common feature in saprolites developed both in tropical and temperate environments. Yttrium produces calculated volume increases of up to a factor of three in the saprolite (Fig. 12b). Such unrealistic increases reflect the loss of Y from the regolith during weathering and emphases the importance of considering a number of inert elements in mass balance calculations (White, 1995).

A unit volume of saprolite v_sp consists of three fractions, the volume of secondary minerals v_sm (e.g., clay and iron oxides), the volume of relatively stable minerals v_i (e.g., biotite and quartz), and the porosity v_ϕ (Cleaves, 1993)

$$v_\mathrm{sp} = v_\mathrm{sm} + v_\mathrm{i} + v_\phi \tag{4}$$

Iso-volumetric weathering in saprolite can be formulated as the rate of downward movement ω_sp (i.e., velocity, m) of the chemical weathering front into the regolith such that

$$\omega_{sp} = \frac{Q_\mathrm{w}}{\rho_\mathrm{p}} \frac{1}{v_\phi} \tag{5}$$

where Q_w is the mass flux of solute transported from the

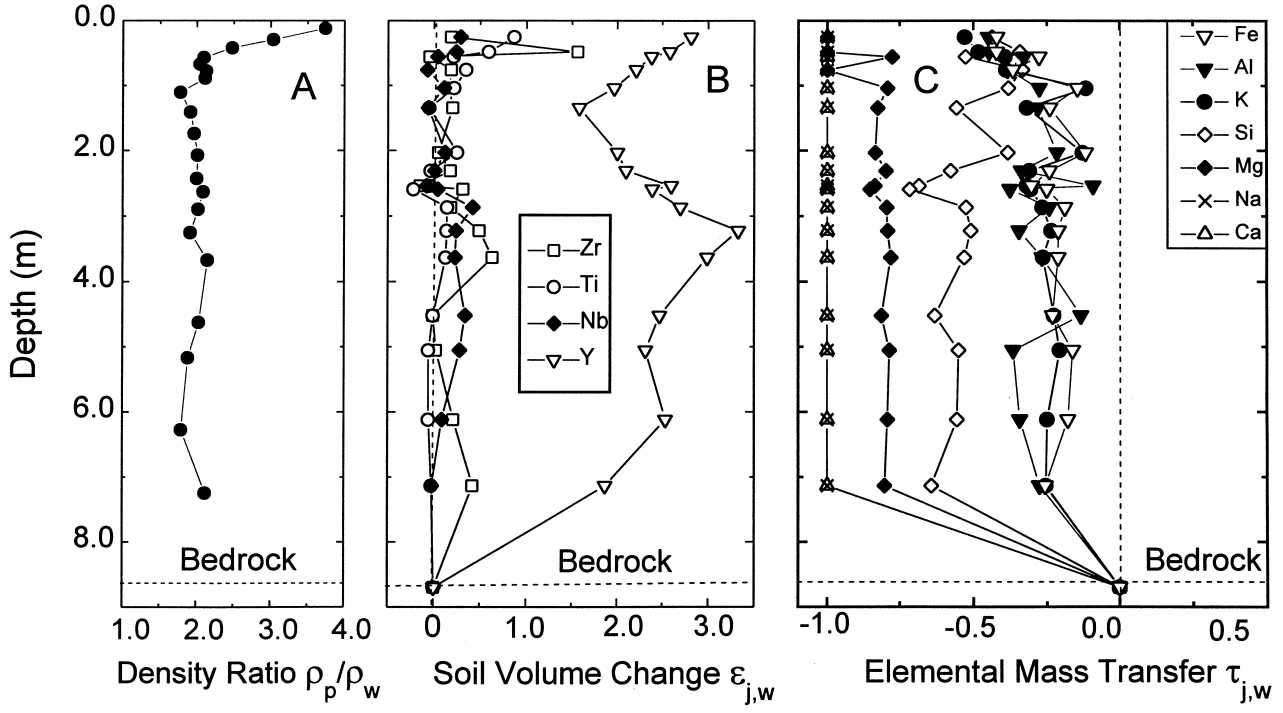

Fig. 12. Weathering characteristics as a function of depth in the ridge top regolith as defined by Eqn 2: (a) Bulk density ratio of prolith to regolith ρ_p/ρ_w, (b) Regolith volume change $\epsilon_{j,w}$ (zero is equivalent to zero volume change), and (c) elemental mass transfer $\tau_{j,w}$ (-1.0 is equivalent to total loss and zero is equivalent to no loss).

weathering profile (kg m^{-2} s^{-1}) and ρ_p is the density of parent rock (2.7×10^3 kg m^3).

Mass flux Q_w from the regolith can be estimated as the difference between total solute discharge at the Rio Icacos gauge and input sources from wet and dry fall and biological fluxes (McDowell and Asbury, 1994). This solute flux (700 kg ha^{-1} yr^{-1}) is normalized to the geographical area of the watershed (326 ha) and converted to a unit surface area of regolith (m^2). The resulting downward propagation rate for saprolite-bedrock interface at the Guaba Ridge site is 58 m Ma^{-1} (Table 6). The propagation rate is significantly faster than for saprolites formed on granitoid rocks in more temperate environments (4–37 Ma^{-1}, Table 6). The rates are higher than average alteration rates of 22 m Ma^{-1} reported (Thomas, 1994) for tropical watersheds underlain by an assortment of rock types and are an order of magnitude faster than the average rate of global weathering based on total river discharge (5.6 m Ma^{-1}; Wakatsuki and Rasyidin; 1992).

The saprolite propagation rate (58 m Ma^{-1}) is similar to the range in denudation rates (25–50 Ma^{-1}) estimated by Brown et al. (1995) from ^{10}Be accumulations on a ridge adjacent to the Guaba Ridge (Table 6). The correlation between weathering velocities and denudation rates supports long term dynamic equilibrium between rates of saprolitization and rates of physical erosion on the ridge crests. A similar conclusion was made by Pavich (1989) in considering denudation rates and saprolite formation in the Occoquan basin of Virginia (Table 6).

5.6. Elemental Mobility in the Regolith

Element mobility in the Rio Icacos regolith is characterized by the mass transfer coefficient τ_j (Eqn. 2) which is computed from density and chemical composition data in combination with volume change derived from the strain calculations

Table 6. Selective weathering and denudation rates for granitoid rocks (m Ma^{-1}).

Rate	Rock	Method	Location	Reference
58	Quartz Diorite	Eqn. 5	Rio Icacos, PR	This paper
25–50	Quartz Diorite	^{10}Be	Rio Icacos, PR	Brown et al., 1995
37	Schist	Eqn. 5	Coweeta, NC	Velbel, 1985
10	Granite	Eqn. 5	Guayana Shield	Edmond et al., 1995
9	Schist	Eqn. 5	Pond Branch MD	Cleaves, 1993
4	Granite	Denudation	Occoquan basin, VA	Pavich, 1986
22	Generic	Alteration	Tropical Average	Thomas, 1994
6	Generic	Denudation	World Average	Wakatsuki & Rasyidin, 1992

Table 7. Weathering fluxes based on changes in regolith chemistry $Q_{j,r}$, infiltration $Q_{j,f}$, and watershed solute budgets $Q_{j,w}$ (units are in moles m^{-2} s^{-1} except as noted).

j	ΔM_j (moles m^{-2})	Δc_j (moles m^{-3})	$Q_{j,r}$	$Q_{j,f}$	$Q_{j,w}$	$Q_{j,f}/Q_{j,r}$	$Q_{j,w}/Q_{j,r}$
Si	1.1 10^5	0.405	1.74E-08	1.38E-08	2.56E-08	0.79	1.47
Na	1.2 10^4	0.128	1.90E-09	4.34E-09	3.45E-09	2.28	1.81
K	4.0 10^3	0.096	8.21E-10	1.10E-09	1.04E-09	1.34	1.26
Ca	1.7 10^4	0.063	2.70E-09	3.25E-09	6.72E-09	1.21	2.49
Mg	6.4 10^3	0.032	1.01E-09	2.13E-09	3.64E-09	2.09	3.59

$$\tau_j = \frac{\rho_w C_{j,w}}{\rho_p C_{j,p}} (\epsilon_{j,w} + 1) - 1 \quad (6)$$

τ_j is plotted for major cations and Si in the Luquillo regolith in Figure 12C. Sodium and calcium are totally depleted during plagioclase and hornblende weathering at the saprolite-bedrock interface ($\tau_j = 0$). Approximately 30% of Mg, and 70% of the K are retained in residual biotite in the saprolite, 40% of the SiO_2 is retained in biotite and kaolinite, and 75% of the Al and Fe are retained in secondary kaolinite and goethite. Elemental losses in the saprolite are essentially constant with depth indicating that a large proportion of the chemical weathering (i.e., loss of Na, Ca, and Si) occurs at the interface between the underlying bedrock and overlying saprolite.

5.7. Comparison of Long and Short Term Weathering Fluxes

Of significant interest in weathering studies is the correlation between rates of long-term weathering based on chemical changes in the regolith and contemporary short-term weathering based on solute infiltration through the regolith or on watershed solute balances. This comparison in the present study will be made in terms of weathering fluxes, defined as the elemental mass transfer per unit area of regolith or watershed surface area per unit time (mol m^{-2} s^{-1}). The term weathering rate will be reserved for the mass loss of a mineral phase defined in terms of specific surface area of that mineral and time (see Murphy et al., 1998). Significant differences between short term and long-term fluxes imply errors in the assumptions used in the weathering calculations and/or fundamental changes in chemical weathering with time (White, 1995). Such differences may be due to climate change (Cleaves, 1993), watershed acidification (April et al., 1986; Kirkwood and Nesbitt, 1991) or other causes.

Long term weathering fluxes in the regolith are defined as

$$Q_{j,r} = \Delta M_j t^{-1} \quad (7)$$

where ΔM_j (moles m^{-2}) is the total mass loss of element j, and t is time (yrs.). The duration of weathering of the Rio Icacos regolith is assumed to be 2.0×10^5 yrs based on ^{10}Be accumulation (Brown et al., 1995). $\Delta M_{r,j}$ is calculated by integrating τ_j (Eqn 2) over depth z (Merritts et al., 1992)

$$\Delta M_{j,r} = \left(\rho_p \frac{C_{j,p}}{m_j} 10^4 \right) \int_{z=0}^{z=d} \tau_{j,w} dZ \quad (8)$$

where d is the total profile depth (8.5 m), ρ_p is the protolith density (2.7 g cm^{-3}), and m_j is the atomic weight of species j (other terms are defined in Eqn. 2). The resulting mass losses $\Delta M_{r,j}$ and corresponding weathering rates $Q_{r,j}$ (Eqn. 7) are tabulated in Table 7 for Si, Na, K, Ca, and Mg.

The corresponding change in mass $\Delta M_{j,f}$ based on solute fluxes in the regolith is calculated by integration of Δc_j (moles m^{-3}), the concentration increase in species j (Eqn. 1), and q_h, the hydraulic flux density (m s^{-1}) over the fluid residence time $*t$

$$\Delta M_{j,f} = -\int_0^{*t} \Delta c_j q_h dt \quad (9)$$

Values for Δc_j, calculated from the sum of mineral contributions from both regolith and bedrock weathering based on the mass balance model (Fig. 11), are tabulated in Table 7.

The hydraulic flux density in Eqn. 9 is given by (Hillel, 1982)

$$q_h = -K_m \nabla H \quad (10)$$

where K_m is the hydraulic conductivity (m s^{-1}) and ∇H is the hydraulic gradient (m m^{-1}). Equation 10 is Darcy's law extended to unsaturated conditions by allowing hydraulic conductivity and pressure head to depend on moisture saturation (S, m^3/m^3). The vertical component of the hydraulic gradient is

$$\frac{dH}{dz} = \frac{dh_g}{dz} + \frac{dh_p}{dz} \quad (11)$$

where z is depth (m), H is the total head (m), h_g is the gravitational head (m), and h_p is the pressure head (m H_2O). By definition, the gravitational gradient, $dh_g/dz = -1.00$. A pressure gradient of $h_p/dz = -1.03$ in the upper portions of the regolith (0.3–1.5 m) is defined by a linear regression fit through the measured tensiometer data (Fig. 4c). The hydraulic gradient ∇H is, therefore, equivalent to -2.03 mm^{-1} (Eqn. 11).

The hydraulic conductivity K_m in the upper regolith at steady-state field conditions is estimated by extrapolating average field saturation at 0.7 m ($S = 85\%$) onto the respective experimental saturation curve for the upper saprolite core (Fig. 5, $K_m = 1.7 \times 10^{-8}$ m s^{-1}). Based on Eqn. 10, the resulting estimated field flux density q_h is 3.4×10^{-8} m s^{-1} (Table 8) which translates to a vertical infiltration rate of approximately 1 m yr^{-1} and a fluid residence time of 8 years. These estimates assume conservation of fluid through out the regolith column, i.e., no evapotranspiration nor lateral flow.

Experimental values of K_m in the overlying soils at 0.32 m are lower than in the saprolite at field moisture saturations (Table 3 and Fig. 5). However, as suggested by the lower Cl concentrations in the underlying saprolite (Fig. 6), significant

infiltration bypasses the soil horizon via animal burrows, root throws and other heterogeneities. In situ conductivities in the soil are significantly faster as verified in tracer tests at the LG-1 site in which LiBr rapidly penetrated through the soil horizon (Turner et al., 1996). The estimated rate of infiltration through the underlying saprolite based on the tracer tests is approximately 2 m yr^{-1} (Table 8).

The resulting solute flux through the regolith is defined as

$$Q_{j,f} = -2.03\,\Delta c_j K_{\mathrm{m}} \qquad (12)$$

Values for $Q_{j,f}$ are tabulated in Table 7 assuming $K_{\mathrm{m}} = 1.8 \times 10^{-8}$ m s^{-1} for unsaturated flow through the upper saprolite.

Elemental fluxes associated with watershed scale weathering $Q_{j,w}$ can be estimated as the differences in fluxes between watershed discharge $Q_{j,\mathrm{dis}}$, wet precipitation $Q_{j,\mathrm{precip}}$ and dry precipitation based a Cl correction where C_j/C_{Cl} is the elemental ratio in sea water (White and Blum, 1995)

$$Q_{j,\mathrm{w}} = Q_{j,\mathrm{dis}} - Q_{j,\mathrm{precip.}} - \left[\frac{C_j}{C_{\mathrm{Cl}}}\right](Q_{\mathrm{Cl,dis}} - Q_{\mathrm{Cl,precip}}) \qquad (13)$$

Normalizing annual average stream discharge (0.38 m^3 s^{-1}; McDowell and Asbury, 1994) over the watershed area (326 ha) produces an estimated infiltration rate of 1.1×10^{-7} m s^{-1} (Table 8). The effect of surface runoff can be further minimized by considering base flow in the stream (0.072 m^3 s^{-1}; Santiago-Rivera, 1992). Base flow during relatively dry periods has a small shallow flow component and is most representative of drainage from the deeper saprolite. The resulting infiltration rate (2.1×10^{-8} m s^{-1}) most closely agrees with the estimated flux density for field saturation in the saprolite (3.4×10^{-8} m s^{-1}; Table 8). The resulting weathering fluxes for base flow (Eqn. 13) are tabulated in Table 7.

Silica weathering fluxes estimated from long term regolith weathering (1.74×10^{-8} moles m^{-2} s^{-1}) is in close agreement with short term weathering fluxes based on regolith infiltration rates (1.38×10^{-8} moles m^{-2} s^{-1}) and base flow in the Rio Icacos (2.56×10^{-8} moles m^{-2} s^{-1}) (Table 7). Silicon is the dominant element released during weathering and is least impacted by other processes, including precipitation inputs and biological cycling. The extent of agreement implies that weathering within the regolith and at the saprolite-bedrock interface are the dominant contributors to watershed Si fluxes. Agreement also supports the contention that although the stable ridge top regolith is not representative of the overall watershed topography, it is representative of the watershed weathering rates. This signifies a chemically limited rather than a physically limited-weathering regime (Stallard and Edmond, 1983).

The ratios of short term to long term cation fluxes $Q_{j,f}/Q_{j,r}$ and $Q_{j,\mathrm{w}}/Q_{j,r}$ are greater than unity (Table 7; 1.2–3.6). Somewhat lower regolith rates are expected based on Eqn. 8, which assumes that all weathering occurs over a discreet interval defined by the depth to the bedrock interface (d = 8.5 m). Undoubtedly some weathering contributions occur from relatively deep fracture systems in the quartz diorite and from surficial weathering of exposed bedrock surfaces on hillslopes and in stream channels. These additional sources are reflected both in the watershed and infiltration mass balances.

The extent of agreement in weathering fluxes is fairly remarkable considering the number of assumptions employed in the calculations. The variables with the largest potential errors are the hydraulic conductivity and flux density (Eqn. 10) which vary by 4 orders of magnitude depending on field saturation (S = 70–100%, Fig. 5). The effect of flux densities on potential Si weathering rates are presented in Fig. 13. The solid circle is the mass loss $\Delta M_{\mathrm{SiO_2}}$ from the regolith over 200 Ka of weathering (Eqn. 8). The upwardly trending lines are weathering trajectories calculated by extrapolation of the solute loss $^*\Delta M_{\mathrm{SiO_2}}$ (Eqn. 9) to long times based on various rates of infiltration (Table 8). Unsaturated flow at average field saturation, when extrapolated to 200 Ka, accurately simulates the Si losses in the regolith $\Delta M_{\mathrm{SiO_2}}$. This weathering rate is bracketed by weathering trajectories calculated from infiltration estimates based on average and base flow from the watershed.

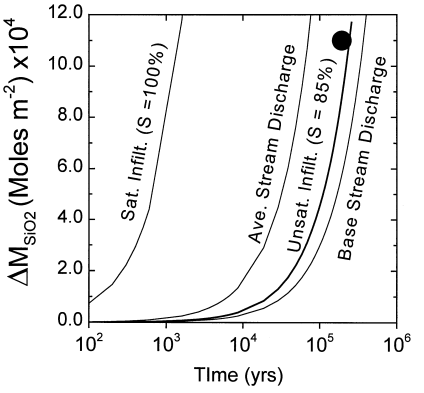

Fig. 13. Comparison of short- and long-term Si weathering rates for the Guaba Ridge saprolite. Solid symbol corresponds to regolith mass loss ΔM_{Si} calculated from changes in chemistry and profile age (Eqn. 8). Lines correspond to weathering trajectories called from solute mass loss $^*\Delta M_{\mathrm{Si}}$ (Eqn. 9) and various infiltration rates (Table 8).

A infiltration rate based saturated conductivity in the upper saprolite is more than 2 orders of magnitude faster than for unsaturated flow (Table 8) and produces a weathering trajectory that simulates the regolith chemical loss $\Delta M_{\mathrm{SiO_2}}$ (solid point) in less than 1.6 Ka. Assuming no surface runoff nor evapotranspiration, annual precipitation (4.2 m yr^{-1}) produces a maximum infiltration rate of 1.3×10^{-7} m s^{-1}. This rate is less than both the saturated K_{m} (5.5×10^{-6} m s^{-1}) and an infiltration rate (4.0×10^{-6} m s^{-1}) determined from slug tests performed in wells completed in saturated saprolite in the Rio Icacos watershed (McDowell et al., 1992; Table 8). In spite of the extremely high rates of precipitation, sustained saturated flow in the regolith is impossible.

Differences in filtration rates illustrates the importance of moisture content on fluid fluxes and corresponding weathering rates, even in very wet tropical climates such as Rio Icacos. In addition to controlling rates of chemical transport during weathering, porewater saturation also influences the wetted surface areas involved in the weathering reactions (Velbel, 1993). Increasing pore water saturation and fluid transport also decreases solute concentrations and chemical reaction affinities which repress the formation of secondary minerals (Nagy et al., 1991) and accelerates the dissolution of primary phases (Burch et al., 1993).

Previous watershed studies have correlated watershed fluxes with changes in regolith chemistry (April et al., 1986; Sver-

Table 8. Estimated infiltration rates (m s^{-1}) and fluid residence times (yrs).

Rate	Time	Method	Reference
5.5 10^{-6}	0.049	Saturated saprolite flux density q_m	This study
4.0 10^{-6}	0.067	Pump test in saturated saprolite	McDowell et al., 1992
1.3 10^{-7}	2.07	Precipitation	McDowell and Asbury, 1994
1.1 10^{-7}	2.45	Annual stream discharge[1]	McDowell and Asbury, 1994
6.3 10^{-8}	4.28	LiBr tracer test	Turner et al., 1996
3.4 10^{-8}	7.93	Saprolite flux density at field saturation, q_m	This study
2.1 10^{-8}	12.83	Base stream discharge[1]	Stantiago-Riviera, 1992

drup, 1990; Kirkwood and Nesbitt, 1991) using less detailed approaches which did not include measured porewater chemistries or the rates of unsaturated flow through the regolith. These studies, generally confined to temperate watersheds impacted by acid deposition, have suggested that present day rates of base cation release may be several times more rapid than long term weathering rates based on mineralogical changes. In contrast, the present study of the pristine Rio Icacos watershed concludes that current weathering rates, based both on solute infiltration rates and watershed fluxes, are indistinguishable from long term rates of regolith weathering. This implies that parameters influencing weathering rates, such as precipitation, temperature, and vegetative cover, while not necessarily constant over the last several hundred thousands of years, have not significantly impacted weathering rates in the Luquillo Mountains of Puerto Rico. This has important ramifications for tropical environments in terms of the possible feedback mechanisms between atmospheric CO_2, rates of silicate hydrolysis, and changes in climate (Berner, 1994; Brady and Carroll, 1994; and others).

6. CONCLUSIONS

Previous descriptions of watershed solute balances have suggested that the Rio Icacos watershed is subjected to one of the fastest chemical weathering rates of granitoid rocks on the earth's surface. The present paper, which emphasizes solute-mineral interaction and transport in the watershed regolith, confirms this conclusion. Weathering occurs in two distinct environments; nearly complete dissolution of plagioclase and hornblende occurs in a thin saprock interface while weathering of biotite and quartz predominates in the overlying thick saprolitic regolith. Fine-grained kaolinite is produced by plagioclase weathering while pseudomorphic replacement of altered biotite by kaolinite occurs in the regolith. These differing weathering environments produce distinctly different water chemistries. Potassium, magnesium, and silicon increase linearly with depth in regolith pore waters. Stream waters are dominated by Ca, Na, and Si. Such differences are atypical of less intense weathering in temperate watersheds. Pore water chemistry in the shallow regolith is controlled by closed system recycling of inorganic nutrients such as K, a common feature in tropical ecosystems.

Iso-volumetric weathering in the saprolite, coupled with watershed solute fluxes, produce a weathering velocity at the saprolite-bedrock interface of 58 m Ma^{-1}, which is in close agreement with denudation rates estimated previously by ^{10}Be analyses. This velocity is an order of magnitude faster than estimates rates of continental weathering. Rates of saprolite formation on ridge tops are consistent with overall watershed weathering rates, implying a chemically limited rather than physically limited weathering environment.

Quantitative estimates of mass loss from the regolith are made based on porosity changes and chemical differences between weatherable and inert elements in the regolith and bedrock. Long term weathering fluxes are calculated from this loss and the estimated age of the regolith surface (200 Ma). Mass losses resulting from solute fluxes are determined using a step-wise infiltration model which calculates mineral inputs to the shallow and deep saprolite porewaters and to stream water. Pressure heads decrease with depth in the shallow regolith indicating that both increasing capillary tension and graviometric potential control porewater infiltration. Experimentally determined hydraulic conductivity measurements produce an infiltration rate of 1 m per year which is in agreement with estimates based on a LiBr tracer test and from base discharge from the watershed. Short-term weathering fluxes are calculated from solute mass losses, the rates of infiltration in the regolith, and from watershed discharge at base flow. A comparison of weathering rates produce close agreement implying that the method for calculating weathering fluxes and the implied assumptions are accurate. Possible changes in patterns of precipitation, temperature, and vegetative cover have not significantly impacted weathering rates in the Luquillo Mountains of Puerto Rico over the last several hundred thousand years. This has important ramifications for tropical environments and global climate change.

Acknowledgments—The authors express their appreciation to Angel Torres-Sanchez of the USGS Puerto Rico District who conducted much of the sampling. The authors also express thanks to Drs. Susan Brantley and Tom Bullen for helpful discussions and to Francoise Guth who performed the SEM and X-ray studies. This work was funded by the U. S. Geological Survey Water, Energy, and Biochemical Budgets (WEBB) program. S. Murphy acknowledges support from grant EAR-8657868 from the National Science Foundation.

REFERENCES

April R., Newton R., and Coles L. T. (1986) Chemical weathering in two Adirondack watersheds: Past and present-day rates. *Geol. Soc. Amer. Bull.* **97,** 1232–1238.

Bain D. C., Duthie M. L. and Miller J. D. (1994) Inorganic nutrient inputs from mineral weathering in two Scottish upland ecosystems. *Appl. Geochem.* **9,** 119–125.

Berggren D. and Mulder J. (1995) The role of organic matter in controlling aluminum solubility in acidic mineral soil horizons. *Geochim. Cosmochim. Acta* **59,** 4167–4180.

Berner R. A. (1994) GEOCARB II: A revised model of atmospheric CO_2 over phanerzoic time. *Amer. J. Sci.* **294,** 56–91.

Boccheciamp R. A. (1977) *Soil survey of the Humacao area of eastern Puerto Rico.* USDA Soil Conserv. Serv.

Brady P. V. (1991) The effect of silicate weathering on global temperature and atmospheric CO2. *J. Geophys. Res.* **96,** 18101–18106.

Brady P. V. and Carroll S. A. (1994) Direct effects of CO_2 and temperature on silicate weathering: possible implications for climate control. *Geochim. Cosmochim. Acta* **58,** 1853–1863.

Brantley S. L., Crane S. R., Creear D., Hellmann R., and Stallard R. (1986) Dissolution at dislocation etch pits in quartz. *Geochim. Cosmochim. Acta* **50,** 2349–2361.

Brimhall G. H. and Dietrich W. E. (1987) Constitutive mass balance relations between chemical composition, volume, density, porosity, and strain in metasomatic hydrochemical systems: Results on weathering and pedogenesis. *Geochim. Cosmochim. Acta* **51,** 567–587.

Brown S., Lugo A. E., Silander S., and Liegel L. (1983) Research history and opportunities in Luquillo Experimental Forest. USDA Forest Serv. Gen. Tech. Rept. SO-44.

Brown E. T., Stallard R. F., Larsen M. C., Raisbeck G. M., and Yiou F. (1995) Denudation rates determined from the accumulation of in situ produced ^{10}Be in the Luquillo Experimental Forest, Puerto Rico. *Earth Plant. Sci. Lett.* **129,** 193–202.

Bruijnzeel L. A. (1990) Nutrient cycling in a moist tropical forests: The hydrological framework. In *Mineral Nutrients in Tropical Forest and Savanna Ecosystems* (ed. J. Procor), pp. 383–415. Blackwell Sci. Publ.

Burch T. E., Nagy K. L., and Lasaga A. C. (1993) Free energy dependence of albite dissolution kinetics at 80°C, and pH 8.8. *Chem. Geol.* **105,** 137–162.

Burnham C. P. (1989) Pedagogical processes and nutrient supply from parent material in tropical soils. In *Mineral Nutrients in Tropical Forest and Savanna Ecosystems* (ed. J. Proctor), pp. 27–40. Blackwell Sci. Publ.

Cappellato R., Peters N. E., and Radsdale H. L. (1993) Acidic atmospheric deposition and canopy interactions of adjacent deciduous and coniferous forests in the Georgia Piedmont. *Canadian J. For. Res.* **23,** 1114–1124.

Chadwick O. A., Brimhall G. H., and Hendricks D. M. (1990) From black box to a gray box: A mass balance interruption of pedogenesis. *Geomorphology* **3,** 369–390.

Chartes C. J., Kirby J. M., and Raupach M. (1990) Poorly ordered silica and aluminosilicates as temporary cementing agents in hard-setting soils. *Soil Sci. Soc. Amer. J.* **54,** 1060–1067.

Cleaves E. T. (1993) Climatic impact on isovolumetric weathering of a coarse-grained schist in the northern Piedmont Province of the central Atlantic states. *Geomorphology* **8,** 191–198.

Dong H., Peacor D. R., Murphy S. F., and Brantley S. L. (1998) TEM study of progressive alteration of igneous biotite to kaolinite throughout a weathered soil profile. *Geochim. Cosmochim. Acta* (submitted).

Durand P., Neal C., Jeffrey H. A., Ryland G. P., and Neal M. (1994) Major, minor and trace element budgets in the Plynlimon afforested catchments (Wales): general trends, and effects of felling and climate variations. *J. Hydrol.* **157,** 139–156.

Eberl D. D., Dritz V. A., Srodon J., and Nüesch R. (1996) Mudmaster: A program for calculating crystallite size distributions and strain from the shapes of X-ray diffraction peaks. USGS Open File Report 96–171.

Eberl D. D., Nüesch R., Sucha V., and Tsipursky S. (1998) Measurement of fundamental illite particle thicknesses by X-ray diffraction using PVP-10 intercalation. *Clays Clay Mineral* (in press).

Edmond J. M., Palmer M. R., Measures C. I., Grant B., and Stallard R. F. (1995) The fluvial geochemistry and denudation rate of the Guyana Shield in Venezuela, Columbia, and Brazil. *Geochim. Cosmochim. Acta* **59,** 3301–3225.

Eswaran H. and Bin W. C. (1978) A study of a deep weathering profile on granite in peninsular Malaysia: II. Mineralogy of the clay, silt, and sand fractions. *Soil Sci. Soc. Amer. J.* **42,** 149–153.

Eswaran H. and Stoops G. (1979) Surface textures of quartz in tropical soils. *Soil Sci. Amer. J.* **43,** 420–424.

Gaillardet J. B., Dupre B., and Allegre C. S. (1995) A global geochemical mass budget applied to the Congo Basin Rivers: Erosion rates and continental crust composition. *Geochim. Cosmochim. Acta* **59,** 3469–3485.

Hamdan J. and Burnham C. P. (1996) The contribution of nutrients from parent material in three deeply weathered soils of Peninsular Malaysia. *Geoderma* **74,** 219–233.

Harden J. W. (1987) Soils developed in granitic alluvium near Merced, California. U.S. Geol. Surv. Bull. 1590-A.

Hillel D. (1982) *Introduction to Soil Physics.* Academic Press.

Hooper R. P., Christophersen N., and Peters N. E. (1990) Modeling stream water chemistry as a mixture of soil water end-members—An application to the Panola Mountain Catchment, Georgia, U.S.A. *J. Hydrol.* **116,** 321–343.

Huges S., Norris D. A., Reynolds B., and Williams T. G. (1994) Effects of forest age on surface drainage and soil solution aluminum chemistry in stagnopodzols in Wales. *Water, Air, Soil Pollut.* **77,** 115–139.

Johnson N. M., Likens G. E., Bormann F. H., and Pierce R. S. (1968) Rate of chemical weathering of silicate minerals in New Hampshire. *Geochim. Cosmochim. Acta* **32,** 531–545.

Jones R. C., Hudnall W. H., and Saki W. S. (1982) Some highly weathered soils of Puerto Rico, 2. Mineralogy. *Geoderma* **27,** 75–137.

Jordon C. F., Kline J. R., and Sasscer D. S. (1972) Relative stability of mineral cycles in forest ecosystems. *Amer. Naturalist* **106,** 237–253.

Karathanasis A. D. (1989) Solution chemistry of fragipan formation: Thermodynamic approach to understanding fragipan formation. In *Fragipans: Their Occurrence, Classification, and Genesis.* (ed. N. E. Smeck and E. J. Ciolkosz); *Soil Sci. Amer. Spec. Publ.* **24,** 113–141.

Katz B. G. (1989) Influence of mineral weathering reactions on the chemical composition of soil water, springs, and groundwater, Catoctin Mountains, Maryland. *Hydrol. Process.* **3,** 185–202.

Kelly J. M. (1988) Annual elemental input/output estimates for two forested watersheds in eastern Tennessee. *J. Environ. Qual.,* 463–468.

Kharaka Y. K., Gunter W. D., Aggarwal P. K., Perkins E., and Debraal J. D. (1988) SOLMINEQ 88: A computer program for modeling water/rock interaction. U. S. Geol. Surv. Res. Invest. Rept. 88-4227.

Kirkwood D. E. and Nesbitt H. W. (1991) Formation and evolution of soils from an acidified watershed: Plastic Lake, Ontario, Canada. *Geochim. Cosmochim. Acta* **55,** 1295–1308.

Klute A. and Dirksen C. (1986) Hydraulic conductivity and diffusivity: Laboratory methods. In *Methods of Soil Analysis* (ed. A. Klute), pp. 687–699. Soil Sci. Soc. Amer.

Larsen M. C. (1997) A study of geomorphic processes and water budgets in the montaine humid-tropical and developed watersheds, Puerto Rico. U PhD thesis, Univ. Colorado.

Larsen M. C. and Torres-Sanchez A. J. (1989) Landslides triggered by Hurricane Hugo in eastern Puerto Rico, September, 1989. *Caribbean J. Sci.* **28,** 113–125.

Larsen M. C., Collar P. D., and Stallard R. F. (1993) Research plan for the investigation of water, energy and biogeochemical budgets in the Luquillo Mountains, Puerto Rico. USGS Open File Rept. 92-150.

Lucas Y., Luizao F. J., Chauvel A., Rouiller J., and Nahon D. (1993) The relation between biological activity of the rain forest and mineral composition of soils. *Science* **260,** 521–523.

McDowell W. H. and Asbury C. E. (1994) Export of carbon, nitrogen, and major ions from three tropical montane watersheds. *Limnol. Oceanogr.* **39,** 111–125.

McDowell W. H., Bowden W. B., and Asbury C. E. (1992) Riparian nitrogen dynamics in two geomorphologically distinct tropical rain forest watersheds; subsurface solute patterns. *Biogeochemistry* **18,** 53–75.

McDowell W. H., Sanchez C. G., Asbury C. E., and Perez R. R. (1990) Influence of sea salt aerosols and long range transport on precipitation chemistry at El Verde, Puerto Rico. *Atmos. Environ.* **24A,** 2813–2821.

Merritts D. J., Chadwick O. A., Hendricks D. M., Brimhall G. H., and Lewis C. J. (1992) The mass balance of soil evolution on late Quaternary marine terraces, Northern California. *Geol. Soc. Amer. Bul.* **104,** 1456–1470.

Meybeck M. (1987) Global chemical weathering of surfical rocks estimated from dissolved river loads. *Amer. J. Sci.* **287,** 401–428.

Millot G. (1970) *Geology of Clays.* Springer-Verlag.

Millot G., Bocquier G., and Paquet H. (1976) Geochimie et payages tropicaux. *La Recherche* **65,** 236–244.

Murphy S. F. (1995) The weathering of biotite in a tropical soil, Luquillo Mountains, Puerto Rico. Master's thesis, Penn. State Univ.

Murphy S. F., Brantley S. L., Blum A., White A. F., and Dong H. (1997) Chemical weathering in a tropical watershed, Luquillo Mountains, Puerto Rico: II. Rate and mechanism of biotite weathering. *Geochim. Cosmochim. Acta* **62,** 229–245.

Nagy K. L., Blum A. E., and Lasaga A. C. (1991) Dissolution and precipitation kinetics of kaolinite at 80°C and pH 3. The dependence on the saturation state. *Amer. J. Sci.* **291,** 649–686.

Nahon D. B. (1991) *Introduction to the Petrology of Soils and Chemical Weathering.* Wiley.

Nimmo J. R., Askin K. C., and Mello K. A. (1992) Improved apparatus for measuring conductivity at low water content. *Soil Sci. Amer. J.* **56,** 1788–1761.

Norfleet M. L., Karathanasis A. D., and Smith B. R. (1993) Soil solution composition relative to mineral distribution in the Blue Ridge Mountain soils. *Soil Sci. Amer.* **57,** 1375–1380.

Pavich M. J. (1989) Regolith residence time and the concept of surface age of the Piedmont peneplain. *Geomorphology* **2,** 181–196.

Plummer L., Prestemon E. C., and Parkhurst D. L. (1991) An Interactive Code (NETPATH) for Modeling NET Geochemical reactions along a flow path. Water Resour. Invest. Repts. 91-4078.

Ramirez A. J. and Andara A. (1993) Water chemistry and chemical weathering in northern Venezuelan drainages. *Chem. Geol.* **107,** 317–318.

Roda F., Avilia A., and Bonila D. (1990) Precipitation, throughfall, soil solution, and stream-water chemistry in a Holm-oak (Quercus ilex) forest. *J. Hydrol.* **116,** 167–183.

Santiago-Rivera L. (1992) Low-flow characteristics at selected sites on streams in Eastern Puerto Rico. USGS Water Res. Invest. 92-4063.

Schoeneberg P. J., Amoegar A., and Buol S. W. (1995) Physical property variation of a soil and saprolite continuum at three geomorphic positions. *Soil Sci. Soc. Amer. J.* **59,** 1389–1397.

Seiders V. M. (1974) Cretaceous and Lower Tertiary stratigraphy of the Gurabo and El Yunque Quadrangles, Puerto Rico. U.S. Geol. Bull. *1294F.*

Simon A., Larsen M. C., and Hupp C. R. (1990) The role of soil processes in determining mechanisms of slope failure and hillslope development in a humid-tropical forest, eastern Puerto Rico. *Geomorphology* **3,** 263–286.

Stallard R. F. and Edmond J. M. (1983) Geochemistry of the Amazon: 2. The influence of geology and weathering environment on dissolved load. *J. Geophys. Res.* **88,** 9671–9688.

Suchet P. A. and J. L. Probst (1993) Modelling of atmospheric CO_2 consumption by chemical weathering of rocks: Application to the Garonne, Congo, and Amazon basins. *Chem. Geol.* **107,** 205–210.

Sverdrup H. U. (1990) *The Kinetics of Base Cation Release Due to Chemical Weathering.* Lund Univ. Press.

Thomas M. F. (1994) *Geomorphology in the Tropics.* Wiley.

Turner B. F., Brantley S. L., Stonestrom D. A., White A. F., and Larsen M. C. (1996) Solute transport and chemical weathering in a tropical rain forest saprolite, Puerto Rico. Geol. Soc. Amer. Natl. Mtg. Abst., Denver, A 131.

Van Wambeke A. (1962) Criteria for classifying tropical soils. *J. Soil Sci.* **13,** 124–132.

Vegas-Vilarrubia T. et al. (1994) Small catchment studies in the tropical zone. In *Biogeochemistry of Small Catchments* (ed. B. Moldan), pp. 343–360. Wiley.

Velbel, M. A. (1986) The mathematical basis for determining rates of geochemical and geomorphic processes in small forested watersheds by mass balance: Examples and implications. In *Rates of Chemical Weathering of Rocks and Minerals.* (eds. S. M. Colman and D. P. Dethier) pp. 439–449. Academic Press.

Velbel M. A. (1993) Constancy of silicate-mineral weathering-ratios between natural and experimental weathering: Implications for hydrologic control of differences in absolute rate. *Chem. Geol.* **105,** 89–99.

Velbel M. A. (1995) Interactions of ecosystem processes and weathering processes. In *Solute Modeling in Catchment Systems* (ed. S. T. Trudgill), pp. 193–211. Wiley.

Vepraskas M. J. and Williams J. P. (1995) Hydraulic conductivity of saprolite as a function of sample dimensions and measurement technique. *Soil Sci. Soc. Amer. J.* **59,** 975–981.

Wakatsuki T. and Rasyidin A. (1992) Rates of weathering and soil formation. *Geoderma* **52,** 251–263.

White A. F. (1995) Chemical weathering rates in soils. In *Chemical Weathering Rates of Silicate Minerals* (ed. A. F. White and S. L. Brantley), *Rev. Mineral.* **31,** 407–458.

White A. F. and Blum A. E. (1995) Effects of climate on chemical weathering rates in watersheds. *Geochim. Cosmochim. Acta* **59,** 1729–1747.

White A. F., Blum A. E., Schulz M. S., Huntington T. G., and Peters N. E. (1998) Mass balance relationships describing rates of chemical weathering and biogeochemical cycling in soil and bedrock environments; Panola Mountain Watershed, Georgia, USA. *Geochim. Cosmochim. Acta* (submitted).

Zarin D. J. and Johnson A. H. (1995) Base saturation, nutrient cation, and organic matter increases during early pedogenesis on landslide scars in the Luquillo Experimental Forest, Puerto Rico. *Geoderma* **65,** 317–330.

Zeman L. J. (1975) Hydrochemical balance of a British Columbia Mountainous watershed. *Catena* **2,** 81–94.